

X-ray emission from early-type stars in the Orion Nebula Cluster

B. Stelzer^{1,2}, E. Flaccomio², T. Montmerle³, G. Micela², S. Sciortino², F. Favata⁴, T. Preibisch⁵ & E. D. Feigelson⁶

stelzer@astropa.unipa.it

ABSTRACT

The X-ray properties of twenty ~ 1 Myr old O, B, and A stars of the Orion Trapezium are examined with data from the *Chandra* Orion Ultradeep Project (COUP). On the basis of simple theories for X-ray emission, we define two classes separated at spectral type B4: hotter stars have strong winds that may give rise to X-ray emission in small- or large-scale wind shocks, and cooler stars that should be X-ray dark due to their weaker winds and absence of outer convection zones where dynamos can generate magnetic fields. Emission by late-type magnetically active companions may be present in either class.

Sixteen of the 20 stars are detected with a wide range of X-ray luminosities, $\log L_x [\text{erg s}^{-1}] \sim 29 - 33$ and X-ray efficiencies $\log (L_x/L_{\text{bol}}) \sim -4$ to -8 . Only two stars, θ^1 Ori D (B0.5) and NU Ori (B1), show exclusively the constant soft-spectrum emission at $\log (L_x/L_{\text{bol}}) \sim -7$ expected from the standard model involving many small shocks in an unmagnetized radiatively accelerated wind. Most of the other massive O7-B3 stars exhibit some combination of soft-spectrum

¹Dipartimento di Scienze Fisiche ed Astronomiche, Università di Palermo, Piazza del Parlamento 1, I-90134 Palermo, Italy

²INAF - Osservatorio Astronomico di Palermo, Piazza del Parlamento 1, I-90134 Palermo, Italy

³Laboratoire d'Astrophysique de Grenoble, Université Joseph-Fourier, F-38041 Grenoble, France

⁴Astrophysics Division - Research and Science Support Department of ESA, ESTEC, Postbus 299, 2200 AG Noordwijk, The Netherlands

⁵Max-Planck Institut für Radioastronomie, Auf dem Hügel 69, D-53121 Bonn, Germany

⁶Department of Astronomy & Astrophysics, Pennsylvania State University, University Park PA 16802, USA

wind emission, hard-spectrum flaring, and/or rotational modulation indicating large-scale inhomogeneity. Magnetic confinement of winds with large-scale shocks can be invoked to explain these phenomena. This is supported in some cases by non-thermal radio emission and/or chemical peculiarities, or direct detection of the magnetic field (θ^1 Ori C).

Most of the stars in the weak-wind class exhibit X-ray flares and $\log L_x < 31 \text{ erg s}^{-1}$, consistent with magnetic activity from known or unseen low-mass companions. In most cases, the X-ray spectra can be interpreted in terms of a two-temperature plasma model with a soft component of 3 – 10 MK and a hard component up to 40 MK. All non-detections belong to the weak-wind class. A group of stars exhibit hybrid properties – flare-like behavior superimposed on a constant component with $\log L_x \sim 32 \text{ erg s}^{-1}$ – which suggest both magnetic activity and wind emission.

Subject headings: open clusters and associations: individual: (Orion nebula cluster) – binaries: general – stars: early-type – stars: pre-main sequence – stars: winds, outflows – X-rays: stars

1. Introduction

Among normal stars, X-ray emission is often strongest in the youngest stellar populations. X-ray emission from OB stars was first reported from observations with the *Einstein* observatory (Harnden et al. 1979; Pallavicini et al. 1981), and dozens were detected with the *ROSAT* All-Sky Survey with characteristic efficiency $\log(L_x/L_{\text{bol}}) \sim -7$ (Berghöfer et al. 1997). Their soft and nearly constant emission was attributed to the integrated emission from a myriad of small shocks due to instabilities in the radiatively-driven outflow (see Lucy & White 1980; Owocki & Cohen 1999; Kudritzki & Puls 2000, for a review of the wind properties of massive stars). Their soft spectrum and mildly variable X-ray emission stood in contrast to the hard and often wildly variable X-ray emission of lower mass T Tauri stars. The variability of these latter stars is attributed to flares resulting from reconnection events in large magnetic loops as in the Sun and other magnetically active stars (Feigelson & Montmerle 1999; Favata & Micela 2003). Thus, early-type stars were viewed to radiate X-rays via a thermal plasma produced by a *thermal* heating mechanism (wind shocks), while late-type stars radiate via a thermal plasma produced by a *non-thermal* heating mechanism (magnetic reconnection flares).

Recent studies by telescopes with sensitivity to hard X-rays and high-resolution spectral capabilities have thrown this simple view into confusion. The brightest star in the Orion

Trapezium cluster, the O7 star θ^1 Ori C, exhibits a hard spectral component and a strong rotational modulation inconsistent with spherically symmetric wind emission. The Trapezium O9.5 star θ^2 Ori A showed a powerful flare superposed on wind-like emission (Feigelson et al. 2002). Spectral lines in these and other O stars are broadened indicating production in the wind acceleration zone, but the line strengths, shapes and absorption often differ from those predicted by the standard wind-shock model (e.g. Miller et al. 2002; Schulz et al. 2003; Cohen et al. 2003). Some of these effects can be attributed to the confinement, and resulting large-scale shocks, of the wind by a strong stellar magnetic field (Babel & Montmerle 1997a; Ud’Doula & Owocki 2002; Schulz et al. 2003). This is supported by the detections of nonthermal radio emission and atmospheric chemical peculiarities in some of these stars.

The X-ray properties of intermediate-mass late B and A stars have also been confusing, but for different reasons. With neither powerful fast winds, nor outer convection zones, no X-rays were expected. Nonetheless, a substantial number are detected with a wide range of X-ray luminosities (e.g. Schmitt et al. 1985; Caillault & Zoonematkermani 1989; Simon et al. 1995; Cohen et al. 1997). In some cases, this emission can be attributed to the presence of low-mass, late-type star companions to the intermediate-mass stars. This was directly demonstrated by resolving several visual binaries with the *Chandra X-ray Observatory* (Stelzer et al. 2003; Behar et al. 2004). But other cases are less clear: some X-ray sources appear to coincide precisely with the B star (Stelzer et al. 2005), and the youngest A and B stars (Herbig Ae/Be stars) sometimes outshine their lower mass companions (Feigelson et al. 2003), perhaps due to star-disk magnetic interactions (Hamaguchi et al. 2005).

These issues can be fruitfully addressed in the Orion Nebula Cluster (ONC) where a roughly coeval population of young stars, covering a variety of early spectral types, can be observed in a single X-ray exposure. With its high spatial resolution and excellent astrometry, *Chandra* is the best instrument for a study of this rich and crowded field. Results from *Chandra* observations carried out in 1999 and 2000 already showed that most OBA stars in the ONC are X-ray emitters¹ above $\log L_t \simeq 28$ erg s⁻¹ (Feigelson et al. 2002; Flaccomio et al. 2003). The luminosities and variability of some OB stars are consistent with wind emission. Similar to findings from earlier X-ray observations, the emission levels are seen to scatter around the canonical $L_x/L_{\text{bol}} \simeq 10^{-7}$ relation. This relation has no immediate physical interpretation but could be recovered in a scaling analysis taking account of the detailed wind-shock structure and wind opacity (Owocki & Cohen 1999). The large scatter of the data around the canonical value has remained unexplained, but may be related to

¹Following Getman et al. (2005a) and other COUP studies, L_t is the X-ray luminosity in the ‘total’ 0.5–8 keV band assuming a distance of 450 pc to the ONC. We later refer to L_s in the ‘soft’ 0.5–2 keV band, and $L_{t,c}$ where the total band luminosity is corrected for absorption.

the fact that L_x and L_{bol} are coupled to each other only indirectly via the wind density parameter M_\odot/v_∞ . Contrary to expectation, the $\simeq 30 M_\odot$ massive Trapezium star θ^2 Ori A exhibited rapid high-amplitude variability characteristic of magnetic flares (Feigelson et al. 2002). Together with other works on early-type stars, these results hint that the X-ray emission mechanism in hot stars is more complex than the simple wind-shock picture outlined above, suggesting in particular that transient magnetic phenomena may be important even in massive stars. In this paper, we seek to clarify these issues and elucidate the respective roles of wind shocks and magnetic activity in the X-ray emission of early-type stars.

Our study of early-type stars in the ONC is based on the nearly-continuous 9.7 day observation of the Orion Nebula made with *Chandra* in 2003. Known as the *Chandra* Orion Ultradeep Project (COUP), this is the most comprehensive X-ray study of a young stellar cluster performed to date. The observation, data analysis, source lists and characteristics are described in detail by Getman et al. (2005a). After describing the sample and presenting its basic X-ray properties (§2), we examine their X-ray spectra (§3) and various types of variability (§4). Section 5 with Appendix A is dedicated to multiple systems, §6 to systems with disks, and Appendix B to a new X-ray detection of an early-type Trapezium star in a crowded region of the field. In the discussion (§7), we confront different possible emission mechanisms for our targets.

2. Early-type stars in the COUP

2.1. Classification

In order to investigate whether or not magnetic phenomena are involved in the X-ray emission mechanisms for the early-type stars of the ONC, we first divide the whole COUP sample of ONC members confirmed by optical spectroscopy (‘optical’ COUP sample) into three groups distinguished by the simplest emission mechanism associated as a class with their spectral types (§1): the hottest stars dominated by wind shocks, the cooler stars dominated by magnetic activity, and an intermediate ‘blank zone’. In this last class no X-rays are expected, because the stars have no, or only a very shallow (outer) convective zone (at most a few percent of the stellar radius; Siess et al. 2000), hence no magnetic activity, and have weak, slow radiative winds or no wind at all. We seek a quantitative basis for dividing these classes here.

In hot massive stars, a radiative force is exerted on heavy atoms in their atmospheres by photospheric ultraviolet photons, transmitting outward momentum to the entire atmosphere via Coulomb collisions (e.g., Kudritzki & Puls 2000). When the radiative acceleration g_{rad}

of the gas exceeds the local gravity g_* , a wind is triggered with net acceleration $g_{\text{rad}} - g_*$. The wind velocity increases up to the sonic point, reaching a ballistic regime with “terminal velocity” $v_\infty > v_{\text{esc}}$, where v_{esc} is the escape velocity of the star. The development of a radiatively accelerated wind thus depends both on a star’s radiation field indicated by its spectral type (or T_{eff}) and its gravity g_* . Metallicity should also play a role but is not considered here, since all stars in our sample are assumed to have the same metallicity.

Early models for radiatively driven winds (e.g., Castor et al. 1975; Abbott et al. 1979) gave a simple, continuous relationship between v_∞ , the mass-loss rate \dot{M} , and T_{eff} , so that the transition between slow winds and fast winds was gradual. However, observations (particularly in the X-ray band) suggest a sharper transition both in v_∞ and \dot{M} around mid-B spectral types. Taking into account the Doppler shifts and shadowing of the photospheric lines, Babel (1996) calculated the locus of the stationary wind regime in the two-dimensional $g - T_{\text{eff}}$ plane. He found that for low temperatures (e.g., $T_{\text{eff}} < 10,000$ K), only weak-gravity stars can have winds, whereas on the main-sequence, for high temperatures ($T_{\text{eff}} > 20,000$ K), winds can exist even for high-gravity stars. In practice, the transition between the weak-wind and fast-wind regimes near the main-sequence takes place for $T_{\text{eff}} \simeq 14,000 - 18,000$ K; i.e., between spectral types B3 and B5 on the temperature scale of Hillenbrand & White (2004).

This choice of boundary between strong and weak winds is supported by two lines of evidence. First, the dependence of v_∞/v_{esc} on T_{eff} saturates at $v_\infty/v_{\text{esc}} \sim 3$ for $T_{\text{eff}} \geq 20,000$ K (Kudritzki & Puls 2000). Second, a simple model of X-ray emission from wind shocks shows a break from $L_x \propto L_{\text{bol}}^1$ to $L_x \propto L_{\text{bol}}^3$ around mid-B stars (Owocki & Cohen 1999), basically due to a rapid change in the opacity of the winds to UV and X-ray photons.

We therefore classify our sample in two groups based on their spectral type range and expected source of X-ray emission:

1. stars with spectral type O through B3 that have strong, optically thick winds (SW),
2. stars with spectral type B5 through A9 that have weak, optically thin winds (WW),

For comparison, we will also make use of the properties of cool, convective stars with spectral type F0 and later that are magnetically active (MA). This physical classification will help us identify and interpret deviations from the simple model predictions outlined in §1.

The coincidence of the lower boundary of the WW stars with the appearance of outer convection zones in cool stars is demonstrated in Fig. 1. It shows the Hertzsprung-Russell diagram with evolutionary interior models by Siess et al. (2000). The jagged curves denote the extent of the convective envelope as a fraction of the stellar radius. The data points

show the ‘optical COUP sample’ of Hillenbrand (1997) (henceforth H97). In all WW stars (shown as large circles), the convective envelopes comprises at most 5 % of the stellar radius.

Roughly two thirds (21/32) of the OBA stars in the ONC are in the field-of-view of the COUP. One star, JW 602, has poorly characterized optical properties (the spectral type is classified as ‘B:’) and is discarded. For the remaining 20 stars, 9 fall in the SW sample and 11 in the WW sample².

Table 1 summarizes stellar parameters for the 20 COUP OBA stars, in order of decreasing effective temperature. We adopt the V magnitude, A_V , and L_{bol} from Getman et al. (2005a), who had extracted the parameters from the original data by H97. When a range of spectral types are present in the literature, a spectral type was assigned corresponding to an estimated average of the group (Hillenbrand, unpublished) and converted to an effective temperature using the scale of Hillenbrand & White (2004). Given the possibility of yet unresolved MA late-type companions, we searched the literature for multiplicity of our targets which is summarized in columns 7 – 9. Finally, in order to investigate the possibility of magnetic star-disk interactions, as in young protostars and T Tauri stars (e.g., Montmerle et al. 2000; Bouvier et al. 1999), we provide in column 10 flags for stars with infrared (IR) excess indicating the presence of circumstellar material.

2.2. X-ray properties

The time-averaged X-ray properties for the 20 stars integrated over the 9.7-day COUP exposure are presented in Table 2. Except for the hardness ratio (column 9), the values are reproduced from the tables of Getman et al. (2005a) who give details of their derivation. The first three columns give the COUP sequence number, the optical counterpart from Table 1, and the spectral type. Following columns provide the off-axis angle and the offset between X-ray source and the near-IR stellar positions. The net source counts in the broad energy band (0.5 – 8.0 keV) after background subtraction and upper limits for undetected sources are given in column 6.

Four of the twenty targets are heavily piled-up in the ACIS CCD detector: COUP 809 (θ^1 Ori C), 1232 (θ^2 Ori A), 745 (θ^1 Ori A), and 732 (θ^1 Ori E). In these cases, only 1 – 4 % of the photons incident on the detector are extracted from an annular region around the

²Two of the WW stars with late-B spectral type have unknown membership probabilities: θ^1 Ori E and θ^1 Ori A. Since B stars are intrinsically rare, we consider it unlikely that these stars are not members of the ONC.

piled-up core of the point spread function (PSF). The spectral and luminosity analysis takes this into account in a self-consistent manner. The luminosity values obtained for heavily piled-up sources are subject to systematic uncertainties of order $\pm 20\%$. The treatment of piled-up COUP sources is described in § 6 of Getman et al. (2005a).

All O to mid-B (SW) stars are detected, including the B2 star Par 1772, a faint X-ray source in a crowded region which had not been detected in previous Orion Nebula X-ray studies (see Appendix A and Fig. 10 for details). Four mid-B to A (WW) stars are undetected: θ^1 Ori F (B8), JW 531 (A1), JW 108 (A3), and JW 608 (A5). None of these stars has exhibited X-ray emission in previous observations. Upper limits to their X-ray luminosities were computed with XSPEC from the counts given in Table 2, assuming an isothermal plasma with energy $kT = 1$ keV, abundance of 0.3 solar, and absorbing column derived from the visual absorptions given in Table 1 according to $N_H[\text{cm}^{-2}] = 1.6 \cdot 10^{21} A_V[\text{mag}]$ (Vuong et al. 2003).

We also list the PSF fraction included in the photon extraction area (column 7), and the effective exposure time (column 8) at that location in the ACIS detector. The PSF fraction is $\sim 90\%$ for most COUP sources, but is lower when the source suffers from pile-up or has a very close neighbor. In such cases, special photon extraction regions have been defined.

The hardness ratio in column 10 is defined as H/S , where H is the number of counts in the hard band ($E > 1.8$ keV) and S is the number of counts in the soft band ($E < 1.8$ keV). This differs from the hardness ratios defined by Getman et al. (2005a). Our choice of the boundary between the hard and soft band is near to the peak of the observed spectrum of our targets, and therefore guarantees a significant fraction of the total collected source photons in each of the bands. In the last column, we provide the number of the respective X-ray source in the previous *Chandra* ACIS observation (Feigelson et al. 2002, hereafter FBG02).

3. Spectral Analysis

We adopt the procedure to extract the X-ray photons described by Getman et al. (2005a), but we conduct a more detailed spectral analysis than their automated fitting procedure, which did not take in account visual absorptions, unusual abundance or temperature distributions, or variability. In addition, as illustrated in their Figure 6, their fits may give incorrect absorption column densities. Our resulting spectral fits to thermal plasma models are summarized in Table 3. X-ray fluxes and luminosities were computed from the spectral fits using the *XSPEC flux* command assuming a distance of 450 pc. We list both the absorbed (L_t) and the absorption-corrected ($L_{t,c}$) luminosities in the 0.5 – 8 keV broad

band.

Spectral modeling was first performed based on a one- or two-temperature plasma in collisional ionization equilibrium using the MEKAL code (Mewe et al. 1985, 1995). Elemental abundances were fixed at $Z = 0.3 Z_{\odot}$ with abundance ratios matching those of Anders & Grevesse (1989). This choice of subsolar abundances follows Getman et al. (2005a), and has been proven appropriate in X-ray studies of various star forming regions (e.g. Nakajima et al. 2003; Feigelson et al. 2002; Preibisch 2003). The spectra of over half of the ONC early-type stars are well-fit by an absorbed, two-temperature (2-T) plasma subject to soft X-ray absorption by a cold intervening medium with column density N_{H} . As noted by Getman et al., in some sources the spectral models are not unambiguous: a large uncertainty is introduced by the choice of N_{H} , resulting in either very cool and heavily absorbed plasma or somewhat hotter plasma subject to light absorption. We have also tested models with N_{H} fixed on the value expected from the Vuong et al. (2003) extinction law, but found after visual inspection of the best fits that the models with free column density are more adequate.

In about half of the sample, the spectral parameters resulting from our analysis are almost identical to those presented in Getman et al. (2005a). Discrepancies for the remaining cases can be attributed to two causes. First, Getman et al. sometimes give parameters of a 1-T model while, to achieve a uniform description of our sample, we prefer the 2-T models. The exception is COUP 995 where the 2-T fits result in lower temperatures and unreasonably high luminosity. Second, the fitting procedure encounters a local rather than global minimum in one of the studies. In these cases, we retain the model which both gives a satisfactory fit ($\chi_{\text{red}}^2 \sim 1$) and has absorption consistent to expected ONC values. That is, the derived column density is neither extremely low ($\log N_{\text{H}} [\text{cm}^{-2}] \leq 20$) nor extremely high ($\log N_{\text{H}} [\text{cm}^{-2}] \geq 22$).

In 4 of the brightest COUP hot stars, no 2-T model provides an adequate description of the observed spectrum. COUP 732 (θ^1 Ori E), 745 (θ^1 Ori A), and 809 (θ^1 Ori C), which all suffer strongly from photon pile-up in the ACIS detector, show a high-energy excess which calls for the inclusion of a third high-temperature component in the model. This high-temperature component does not significantly affect the derived luminosity. For θ^1 Ori C (COUP 809), the brightest X-ray source in the field, substantial discrepancies between best-fit model and data are left, which may be related to residual pile-up in the extracted area and/or uncertainties in the response for the annular extraction region. Since our modelling did not improve the result for COUP 809, we use the spectral parameters given by Getman et al. (2005a), but caution that the luminosity might be overestimated (see § A.1).

The emission measures for the soft (EM_1) and hard (EM_2) components of the 2-T fits are compared in Figure 2. There is a general tendency of the WW stars to show $EM_2/EM_1 > 1$,

and of the SW stars to show $EM_2/EM_1 < 1$. Some SW stars – θ^2 Ori A, NU Ori and to lesser extent Par 1772 – are very strongly dominated by the soft component.

In addition to this plasma modelling procedure, we examined a simple model-independent spectral measure using the hardness ratio. The median values of HR for the three subsamples are: $\langle HR \rangle_{MA} = 0.37$, $\langle HR \rangle_{WW} = 0.29$, and $\langle HR \rangle_{SW} = 0.18$. Nonparametric two-sample tests indicate that the difference in HR distributions for SW stars and MA stars is significant at the $P < 1\%$ confidence level, while WW and MA stars are statistically indistinguishable.

4. Variability

4.1. Statistical tests

Variability is a characteristic property of magnetically active low-mass pre-main sequence stars (Montmerle et al. 1983). Strong variations of their X-ray output are observed on short timescales (minutes to hours), while longterm variability is less pronounced and may be the result of catching the star during different phases of short-term events. Studies of X-ray variability on short timescales in hot wind-driven stars are practically absent in the literature. But comparing different sets of observations for a given star has provided little or no evidence for long-term variations (Berghöfer et al. 1997), leading to the conviction that hot stars show no X-ray variability. In this vein, variability can be an important diagnostic for discriminating the origin of the X-ray emission in wind shocks *vs.* magnetic activity. On the other hand, to our knowledge no study has been performed where the variability of hot and cool stars was directly compared in a consistent manner. This is the purpose of this section.

The observable variable phenomena include flares of different morphology, rotational modulation, and irregular variations on short and long timescales. For subsamples of COUP stars detailed variability studies are presented by Favata et al. (2005); Flaccomio et al. (2005); Wolk et al. (2005). Classification of a given event into any of the above mentioned categories of variability is not straightforward. Especially the definition of a flare, generally viewed as an event with rapid rise and spectral hardening followed by decay and spectral softening, escapes consensus on its quantitative description throughout the literature.

We apply here a method described by Wolk et al. (2005) for analysis of flare-like variability in COUP MA sources. It is based on Maximum Likelihood Blocks (MLB), a modification of Bayesian Blocks developed by Scargle (1998), in which the X-ray lightcurve is divided into contiguous segments of constant signal. The segmentation algorithm has two

free parameters: the minimum number of counts accepted in a given segment and the significance, defined as the probability that a constant lightcurve is spuriously segmented due to random fluctuations. In this study of OBA COUP stars, we set a minimum segment of 20 counts and a significance for change points of 95 %.

The results of the variability tests are summarized in Table 4. Stars are sorted in order of decreasing effective temperature. Columns 4 and 5 flag stars variable according to a simple Kolmogorov-Smirnov (KS) test and the MLB test. The KS-test shows 12 out of 16 targets are variable at the 95 % confidence level. The MLB test indicates 14 of our targets can not be described with a single block and thus are likely variable.

The ML blocks are also used to define a ‘characteristic level’ and flares, represented by periods of ‘very elevated’ count rate and rapid flux change as quantified by the derivative of the lightcurve (Wolk et al. 2005). A total of 15 flares are identified, distributed among the 20 targets as summarized in column 6 of Table 4. Columns 7 and 8 give the fraction of the time spent in the ‘characteristic level’ ($t_{\text{char}}/t_{\text{total}}$) and the ratio between the count rate of the highest segment and the ‘characteristic level’ ($R_{\text{peak}}/R_{\text{char}}$). In Figure 3, the amplitude of the lightcurve variations, $R_{\text{max}}/R_{\text{min}}$ is compared to that of COUP low-mass MA stars. Stars for which the maximum count rate corresponds to a flare are distinguished by filled plotting symbols. The amplitudes clearly indicate that SW stars are less strongly variable than MA stars.

The sensitivity to the detection of variability depends on the signal-to-noise. Fig. 4 shows the fraction of variable stars for different count levels. The curves represent COUP MA stars. The solid line is for the KS-test and the dashed line for the MLB test. The total number of stars in each bin is indicated on top of the graph. These data demonstrate that nearly all X-ray-bright low-mass stars are found to be variable. An equivalent study for the SW and WW stars is prohibited by the small number of objects in our sample. Instead, we place the SW and WW stars on the MLB and KS curves for MA stars, at the position corresponding to their observed counts. From this comparison, we find that 96% of WW and SW stars are expected to be variable. For the WW, this is consistent with the observed fraction of 100% variable stars. The fraction of variable WW stars is thus similar to that of MA stars. But for the SW stars, the expected variable fraction is somewhat higher than the observed fraction of 78% variable stars (see Table 4). A deficiency of SW variability is also suggested by the fact that only 4 flares appear in 9 SW stars compared to 11 flares in 7 detected WW stars.

4.2. Flares

The lightcurves of all detected targets are shown in Fig. 5 together with the time evolution of the hardness ratio evaluated in each segment of the MLB test. Signatures of heating during phases of increased intensity are obvious support for the interpretation of these episodes as magnetic reconnection flares. In the following, the characteristics of the flares on SW and WW stars are compared to the flares on solar-mass COUP stars presented by Wolk et al. (2005) which uses the same MLB and flare characterization methodology. Since only 4 flares were observed on SW stars, we did not compute statistics for this group alone, but rather examine how the derived values for WW stars change if we combine the sample with the SW stars. Spectral analysis is based on two-temperature plasma fits of flare segments (see § 3) for the 12 (9) flares in the SW+WW (WW) samples where >50 counts were collected. The results of this comparison are summarized in Table 5.

A histogram showing the distribution of flare durations for the WW stars is given in Figure 6. Although the median of the flare duration on WW stars is only about 1/3 of the value for solar analogs, the distribution seems to be roughly in agreement with the $0.1 \times e^{(-t/100 \text{ ks})}$ relation that describes the distribution for solar-type stars. Following the arguments of Wolk et al. (2005), we derive a flare frequency of 1 flare every 710 ks for WW stars which is similar to the value of 1 flare every 640 ks obtained for ONC solar analogs. For SW stars, the flare frequency is three times lower at 1 flare every ~ 2200 ks.

The median flare luminosity and energy of WW stars is similar to the respective values for solar-type stars, while in the total sample of SW plus WW stars both the flare luminosity and energy are increased by almost 1 dex. A possible interpretation is that the flares of SW stars are *not* drawn from the population of COUP MA stars, but are the result of a different emission mechanism. Since the sudden energy release observed in flares points at the presence of magnetic fields one possible explanation for the flares on SW stars is that they arise from magnetically mediated events in the strong winds. Note, however that the flares on SW stars are not particularly strong with respect to the characteristic level; their high luminosities are due to the overall higher emission level of SW stars with respect to the WW and solar-type stars. The different quiescent luminosity of the SW stars and WW stars may give rise to a bias, because smaller flares are more difficult to detect on brighter stars. Indeed, if we examine the individual events, the strongest flares on SW stars are comparable to the strongest flares on WW stars and solar-type stars, at odds with the above mentioned interpretation. A thorough quantitative comparison of COUP spectra/variability and the MCWS model can be obtained with help of simulations, but it is beyond the scope of this paper and will be addressed in a future study.

4.3. Rotational Modulation

Rotational modulation of the X-ray signal is expected if the X-ray emission is concentrated in long-lived inhomogeneous magnetic field structures, such as active regions on a MA star or the magnetosphere in a magnetically confined wind shock (MCWS). However, since the X-ray emitting plasma is optically thin, rotational modulation may exist only as a result of asymmetries along the line of sight: stellar occultation (provided the emitting volume is not much larger than the star), or non-spherically symmetric absorbing material such as the ‘cooling disk’ of the MCWS model.

In contrast to the optical band where rotational patterns related to active regions are readily observed in many late-type stars, reports on rotational modulation in the X-ray band have been scarce due to inadequate time coverage of past observations. The rotation periods of active late-type stars are on the order of $\sim 1 - 10$ days, accessible to the 13.2 days spanned by the COUP exposure but longer than previous X-ray exposures of pre-main sequence stars.

Flaccomio et al. (2005) detect rotational modulation in $\simeq 10\%$ of a subgroup of > 200 COUP stars examined systematically, which definitely is the biggest sample studied in this respect to date. They compute the Lomb Normalized Periodogram (Scargle 1982) on binned COUP lightcurves. The peak frequencies in the periodogram are then identified and a False Alarm Probability (FAP) is computed using Monte Carlo techniques allowing for correlated noise. The analysis is made both on the original data and on lightcurves trimmed of bright flares. We now apply these methods to the ONC early-type star sample.

We examine the COUP lightcurves of the three stars in the SW and WW sample which have photometrically measured rotation periods: θ^1 Ori C, JW 660, and JW 165. Two additional stars, JW 831 and JW 531, were surveyed for starspot induced photometric variability by Choi & Herbst (1996), but no period was found. At the present stage we discuss only stars with known optical period, because the search for X-ray periods is complicated by flares and other types of variability. A systematic analysis of the whole COUP sample with known optical period (Flaccomio et al. 2005) has shown that sometimes the X-ray period does not coincide with the optical one, suggesting that the complex X-ray lightcurves can result in spurious periods. Our results for the three stars analysed here are summarized in Table 6, and phase-folded lightcurves and hardness ratios can be found in Fig. 7. The median count rate and the amplitude (columns 5 and 6 of Table 6) were computed from the folded lightcurve. The uncertainty of the amplitude derives from the scatter of the data near maximum and minimum, and thus takes into account the intensity changes from one cycle to the other.

4.3.1. θ^1 Ori C = COUP 809

An optical period of 15.43 d was reported by Stahl et al. (1993), and also evidenced in a set of 10 *ROSAT* X-ray observations separated by ~ 2 days each, such spanning a little more than one cycle (Gagné et al. 1997). The same variability pattern is recovered in the COUP lightcurve (Fig. 7). The X-ray lightcurve is almost exactly in phase with the H α ephemeris measured 10 years earlier, and the X-ray period agrees remarkably well with the optical period. The X-ray hardness ratio varies out of phase with the intensity by roughly half a cycle. While there is a concern that incomplete correction for photon pile-up in the ACIS detector may be responsible for the variation of the hardness ratio, we believe this is not occurring. If this were the case, one would expect a correlation with the lightcurve and not an anti-correlation because the increased pile-up during higher intensities would shift photons into the high-energy portion of the spectrum.

Astrophysical discussion of this source in the context of detailed evidence for an inclined dipole field in θ^1 Ori C and magnetically trapped wind plasma (e.g. Babel & Montmerle 1997a; Donati et al. 2002; Schulz et al. 2003; Smith & Fullerton 2005) will be the subject of a forthcoming study.

4.3.2. JW 660 = COUP 1116

A rotation period of 6.15 d was reported by Choi & Herbst (1996) and Herbst et al. (2000) for this B2.5 star, although the cause of a spot pattern on an early-B star is not clear. We find two episodes of enhanced count rates in the COUP lightcurve, which may define an X-ray period of 6.67 d (Fig. 7). The amplitude of the folded lightcurve is poorly defined due to the different peak intensity in the two consecutive cycles. It is also possible that the two features are long-duration flares unrelated to any rotating structures. The hardness ratio varies in phase with the brightness of the source. Spectral hardening during phases of higher intensity is a typical signature of magnetic activity and is opposite to the pattern seen in θ^1 Ori C.

More detailed information on the run of temperature and emission measure is obtained from time-resolved spectroscopy. The spectrum of JW 660 can be described adequately by a two-temperature thermal model with comparatively high temperature at all phases of the presumed rotation cycle. These fits require an absorbing column somewhat higher than the value inferred from the optical extinction. During the maximum of the cycle the higher temperature is slightly enhanced and the emission measure shifted towards the hot component, in agreement with the evolution of the hardness ratio. A feature from highly

ionized iron at ~ 6.7 keV is pronounced during the phase of maximum brightness. Its appearance results from improved statistics rather than a true change in the spectral shape.

4.3.3. *JW 165 = COUP 113*

A photometric period of 5.77 d was reported by Herbst et al. (2000) for this A7 star, albeit based on a single observing season. The period search on the COUP data results in a period of 4.6 d, but the folded X-ray lightcurve is rather noisy (Fig. 7). Spectral fitting suggests a soft X-ray absorption inconsistent with the visual extinction.

5. Multiple Systems

About half of our sample has been carefully examined for multiplicity using traditional spectroscopic and newer speckle and adaptive optics imaging techniques, as indicated in columns 7–9 of Table 1. High-multiplicity visual systems are common among the ONC OB stars, and we summarize known components of our sample stars in Table 7. In all cases the primary falls into the SW category, and most of the secondaries seem to be WW stars rather than MA stars. However, the mass estimates are often based on photometry and have large uncertainties. We also caution that additional, faint lower-mass companions may be present which could contribute to the X-ray emission. Recall that $1''$ separation corresponds to a projected distance of 440 AU. Five well-characterized systems are presented in Appendix A where we discuss the characteristics of their X-ray emission with the aim to identify the X-ray emitting component.

Only one of these multiple systems is resolved in the COUP: the quintet θ^1 Ori B consists of two X-ray sources (Fig. 8, see Appendix B for details). θ^1 Ori B East (COUP 778) emits $\log L_{t,c} = 30.1$ erg s $^{-1}$ with an unusually soft spectrum and no strong variability. This source can be plausibly attributed to wind shocks of the B2.5 primary. In contrast, θ^1 Ori B West (COUP 766) has all the characteristics of a MA lower-mass member of the Orion population with several flares. It is not clear which of the components of the θ^1 Ori B West binary is the principal X-ray emitter.

6. Stars with evidence for disks

Our sample includes four stars listed in the catalog of Herbig Ae/Be stars by Thé et al. (1994) in their Table 5 labelled ‘non emission line early-type shell stars and young stellar

candidates’. Stars in this table lack emission line signatures of accretion, thus do not satisfy the classical definition of HAeBe stars as emission line objects, but IR photometric excesses were seen with *IRAS*. A dust shell is identified around one additional star of our sample (Tovmassian et al. 1997, see flag for *IRAS* excess stars in the last column of Table 1). The *IRAS* measurements indicate that a substantial amount of the luminosity of these stars is irradiated in the far-IR, probably related to dust emission at 100 – 1000 AU from the star. Par 1772 and V361 Ori are discussed by Manoj et al. (2002) who estimate dust masses between those of typical HAeBe stars and of Vega-like stars. The absence of emission features in the spectrum of Par 1772 and JW 153 was confirmed by Böhm & Catala (1995), thereby showing that the accretion phase has ended in these objects.

Figure 11 shows the near-IR color-color diagrams for our sample. For those stars detected in the COUP the *JHKL* magnitudes are reported by Getman et al. (2005a) while for the nondetections we compiled IR photometry from the 2MASS database and the literature (Hillenbrand et al. 1998; Carpenter et al. 2001; Muench et al. 2002). No strong indications for excess emission above the photosphere is seen in the *JHK*-diagram, but several stars have *L*-band excesses. A comparison to the intrinsic IR colors of a late-type star shows that the redder color expected from the presence of a hidden cool star can not account for the observed excesses. We conclude that the near-IR excesses must be ascribed to circumstellar material. We note that the five *IRAS* excess stars do not show stronger *K* – *L* excess than the remaining sample. This suggests they have evolved disks where the inner, hotter part has been cleared.

We find no link between X-ray properties and the presence or absence of an IR excess. For example, a wide spread $-8 < \log(L_x/L_{\text{bol}}) < -5$ is seen among the stars with evidence for disks, which does not favor a common origin of their X-rays (Figure 12). One of the five *IRAS* excess stars, JW 531, remains undetected in the COUP.

7. Discussion

7.1. COUP results in perspective

The COUP is the most sensitive X-ray image ever obtained of a rich young (~ 1 Myr old) stellar cluster with an initial mass function extending up to $\simeq 45 M_\odot$, providing the opportunity to study the X-ray emission of a coeval sample of early-type stars on a long continuous time baseline. The X-ray emission mechanisms of early-type stars are highly disputed (§1). In the hotter stars, our SW sample, the stellar winds most likely play a crucial role. About half of the SW sample is dominated by soft X-rays that are likely

generated by a myriad of small shocks produced by instabilities in their line-driven winds (Lucy & White 1980; Owocki & Cohen 1999). The other half, mostly the B1 to B3 type stars, the cooler stars in the SW sample, also show substantial hard emission, unexplained within the wind-shock model. This emission may indicate that magnetic fields are involved.

Direct observational evidence for the existence of magnetic fields on early-type stars is scarce and mostly restricted to the class of CP stars (Landstreet 1992). On the other hand, magnetic fields are often held responsible for imposing the cyclic variability of wind properties observed in the UV (e.g. Kaper et al. 1999; de Jong et al. 2001) and for the non-thermal radio emission seen in some O stars (Abbott et al. 1984; Van Loo et al. 2004). While traditionally magnetic fields on hot stars are believed to be fossil remnants of the star formation process, numerical modelling has shown that dynamos may operate in their convective cores (Charbonneau & MacGregor 2001). However, the theory has difficulties transporting magnetic flux throughout the thick radiative layer to the stellar surface (MacGregor & Cassinelli 2003). Hybrid models including winds disturbed in large-scale magnetospheres have been developed to explain both radio and X-ray emission from early-type stars (Trigilio et al. 2004).

These models have two implications for the mechanism of X-ray production. First, X-ray emission may be produced as a result of magnetic reconnection in the current sheet that forms in the equatorial plane where gas pressure opens the field lines. This model explains the observed non-thermal radio emission of magnetic CP stars (Linsky et al. 1992), and Usov & Melrose (1992) have estimated that the expected X-ray luminosities are $\log L_x \sim 31 - 34 \text{ erg s}^{-1}$. Therefore, gas heating by magnetic reconnection or other instabilities at the equatorial current sheet from a dipolar field of an early-type star can account for X-ray emission from radiative stars; i.e., both SW and WW stars. Second, in the magnetically confined wind shock (MCWS) model (Babel & Montmerle 1997a), the major effect of the magnetosphere is to confine and channel the wind to the equatorial plane where a quasi-stationary large-scale shock forms. The cooling of shocked material results in the formation of a ‘cooling disk’, partially absorbing the emitted X-rays and periodically modulating the observed X-rays. This model can explain the high temperatures and unusual X-ray line shapes seen in θ^1 Ori C (Schulz et al. 2003; Gagné et al. 2005).

In less luminous WW stars, the wind velocities are smaller than in SW stars. Production of X-ray emission in small-scale wind shocks becomes questionable although the MCWS model may still apply; indeed, this model was first devised for the magnetic Ap star, IQ Aur (Babel & Montmerle 1997a). Perhaps the most common explanation for the X-ray emission from WW stars – applicable to the weaker SW stars as well – invokes unknown or unresolved late-type companions (separations smaller than ~ 100 AU). Such objects would by their

nature be magnetically active (MA), and produce relatively hard, highly variable X-ray emission with typical luminosity between $\log L_x \simeq 28 - 31 \text{ erg s}^{-1}$.

Distinguishing between the different possible emission scenarios based on observational facts is not straightforward. In this section, we use the results from the COUP to test our *a priori* division of the early-type stars in the ONC into SW and WW stars, and we provide a tentative classification of all targets. This classification scheme involves three criteria – X-ray luminosity, spectrum, and variability – and is summarized in Table 8.

7.2. Classification of ONC early-type stars X-ray emission

We consider first Fig. 12 which plots the L_x/L_{bol} ratio against the effective temperature for the SW and WW stars in the COUP. For both groups of stars, a wide spread of L_x/L_{bol} ratios is seen without dependence on T_{eff} . The WW stars show a very wide spread around $\log(L_x/L_{\text{bol}}) \sim -5$ to -6 . The SW stars do not cluster near the empirical relation $\log(L_x/L_{\text{bol}}) \simeq 10^{-7}$ reported in earlier observations of X-ray emission from hot stars and interpreted in terms of the standard wind-shock model (Sciortino et al. 1990; Berghöfer et al. 1997). They scatter by more than two dex around this level.

Nonetheless, we use this $L_x - L_{\text{bol}}$ scaling relation to help classify and understand the X-ray emission of ONC early-type stars. We compare the observed luminosities $L_{\text{t,c}}$ to the ‘predicted’ luminosity $L_{\text{x,p}} = 10^{-7} L_{\text{bol}}$ for stars of the SW class. For the WW class, we use a ‘predicted’ luminosity $L_{\text{x,p}} = 10^{-4} L_{\text{bol}}$ which is characteristic of lower-mass MA stars (Preibisch et al. 2005). These levels are shown as dotted lines in Figure 12. Since MA companions are likely to have L_{bol} lower than the primary, this $L_{\text{x,p}}$ is actually a lower limit. In column 4 of Table 8, we distinguish the following situations:

If $L_{\text{t,c}}/L_{\text{x,p}} < 10$, the emission mechanism defined above for the SW and WW stars respectively is considered to be the dominating mechanism. We denote this mechanism in column 4 by “W” for wind-shock and “T” for T Tauri-like magnetic activity. Note that, in the latter case, as an alternative to a MA late-type companion, the emission might be due to a magnetic reconnection process in a wind.

If $L_{\text{t,c}}/L_{\text{x,p}} > 10$, a different or additional mechanism is considered to be present. We denote this situation by a “>” sign in column 4.

In column 5 of Table 8, we summarize the result of the X-ray spectral analysis (§3) for all detected stars. We consider the X-ray spectrum characteristic for small-scale wind shocks if the soft component (with $T \sim 2.5 \text{ MK}$) of the two-temperature fits dominates the

emission measure (see Figure 2), or if a hard component is altogether absent. Such sources are denoted by “W”. We see a clear pattern that such soft-dominated spectra are seen only in some SW stars and not in any WW stars.

Column 6 tabulates results of the variability analysis (§4) based on the COUP light curves. Constant or weakly variable light curves characteristic of small-scale wind shocks are denoted “W”. Flare-like high-amplitude variability indicates magnetic reconnection (“T”), which might be either from lower-mass MA T Tauri companions or from large-scale shock events in a magnetically confined wind. Smooth lightcurves (“S”) indicate non-flare-like variability such as periodic modulations with moderate amplitudes (factors $\sim 2 - 3$).

In column 7, we categorize the observational indications for the presence of circumstellar material (§6). Recall that no emission-line stars (= HAeBe stars) have been identified in the ONC, but some evidence for disks is seen in the near-IR color-color diagrams or in far-IR fluxes. Finally, column 8 collects observational evidence for magnetic fields including rotational modulations (RM), non-thermal cm radio emission (NT), chemically peculiar characteristics (CP), or direct indicators such as by Zeeman or polarization measurements (B).

Some immediate conclusions may be drawn from Table 8 and the underlying findings presented throughout this paper:

1. There is a clear distinction between the higher-mass SW and all WW stars in terms of their X-ray properties. This justifies *a posteriori* our adopted division between SW and WW classification. However, the location of the transition between the two classes remains ill-defined and may be earlier than the B4 boundary adopted in § 2.1. Some B0–B3 stars have luminosities consistent with X-ray production in the wind, but have spectra and variability characteristics of magnetic activity.
2. In the more massive SW stars with spectral types B0–O7, small-scale wind shocks predicted by the original model of Lucy & White (1980) appear to be the dominant X-ray emission mechanism. But even here, magnetic processes seem to be present; e.g., to explain the powerful $L_x \sim 10^{32}$ erg s⁻¹ COUP flare in θ^1 Ori A (Figure 5), and a similar flare in θ^2 Ori A seen in the earlier *Chandra* study of Feigelson et al. (2002). If one includes the rotational modulation of θ^1 Ori C and the X-ray independent indicators of magnetic fields, all three of the most massive Trapezium stars – θ^1 Ori C, θ^2 Ori A and θ^1 Ori A – show hybrid wind/magnetic characteristics; see Schulz et al. (2003) for a discussion of these hybrid systems in the Orion Nebula hot stars. These stars are promising candidates for the MCWS model.
3. The less massive SW stars similarly show hybrid characteristics combining winds and

magnetic activity. Here the X-ray luminosities are lower, $L_x \simeq 29 - 31 \text{ erg s}^{-1}$, as expected for lower-mass T Tauri companions, and evidence for magnetic fields is found in some but not all objects. Interestingly, most SW stars with emission above the canonical line of $\log(L_x/L_{\text{bol}}) = -7$ are known to have lower-mass companions that are unresolved in X-rays.

4. In the WW class, the X-ray emission is either undetected with very sensitive limits ($L_x/L_{\text{bol}} < 10^{-7}$), or is detected with properties associated with magnetic activity from a late-type companion.
5. Objects with circumstellar disk indicators show no evidence for a common X-ray emission mechanism. We conclude that disks do not play a significant role in the X-ray emission of the early-type ONC stars.

We will now discuss the sample stars in more detail, starting with the cooler intermediate-mass WW stars and proceeding to the SW stars.

7.3. WW stars

The situation for the ONC WW stars (i.e., spectral types B5 and later) seems fairly straightforward (Table 8). Out of 11 stars, 4 are not detected with upper limits several orders of magnitude below the activity level and clearly lower than the L_x of all detected WW stars (see Fig. 12). A bimodal distribution of X-ray luminosities for B- and A-type stars has been suggested in other studies (Preibisch & Zinnecker 2001; Feigelson et al. 2002; Stelzer et al. 2003), explained by zero emission by the intermediate-mass stars and emission by lower-mass MA companions when present. Our data can not distinguish between two separate populations and a single population with a very wide dispersion.

The X-ray luminosities of the majority of the detected WW stars range between $\log L_x [\text{erg s}^{-1}] \sim 29 - 31 \text{ erg s}^{-1}$, typical of ONC late-type MA stars (Feigelson et al. 2005; Preibisch et al. 2005), and therefore consistent with the unresolved binary companion hypothesis. Our study of their variability in general and flaring in particular, and their spectral hardness support the identification of WW X-ray emission with late-type MA companions. Not enough is known about $\theta^1 \text{ Ori BW}$ to assign an X-ray emission mechanism, although the flare-like variability suggests the possible presence of an MA companion. Remarkably, none of the WW stars in the COUP sample is a known multiple; the multiple systems discussed in Appendix A are all SW stars. However, this is most likely due to a lack of systematic binarity searches in the WW population.

The WW star θ^1 Ori E (B5) has unique properties in the COUP data. It has a much higher time-averaged X-ray luminosity than the other WW stars, $\log L_{t,c} = 32.4$ erg s $^{-1}$ and $\log(L_{t,c}/L_{bol}) = -3.6$ (Table 3). Its $\log(L_x/L_{bol})$ level is several orders of magnitude above any standard wind-shock prediction. This star also shows evidence for non-thermal radio emission (Felli et al. 1993), and Schulz et al. (2003) found plasma temperatures ranging from 4 to 47 MK in a study of *Chandra* grating observations. Therefore, it may have an extended magnetosphere, able to confine its weak wind within the MCWS framework. θ^1 Ori E has also shown a flare, which – if attributed to a late-type MA companion – would be one of the most powerful flares seen in any T Tauri star (Grosso et al. 2004; Favata et al. 2005). Altogether, the COUP properties of θ^1 Ori E are not easily explained in a coherent fashion.

The X-ray properties of the A7 star JW 165 are also worth noting. Its smooth lightcurve is consistent with both rotational modulation or slow flares. Its late spectral type implies that its wind must be very weak. For comparison, the calculations by Babel & Montmerle (1997a) for IQ Aur, a hotter A0 star, give $\dot{M} \sim 10^{-10} M_\odot \text{ yr}^{-1}$. JW 165 may have an unseen magnetosphere, although in this case its mass-loss rate should be $\dot{M} > 10^{-12} M_\odot \text{ yr}^{-1}$ since it is not known to be CP. Perhaps more likely, it has a MA T Tauri companion responsible for the emission and peculiar variability observed during the COUP exposure.

7.4. SW stars

Based on the emission diagnostics in column 4 of Table 8, the SW stars can be subdivided in two groups: (i) those for which the X-ray luminosity is consistent with small-scale wind shock emission, and (ii) those which are overluminous by one or two orders of magnitude with respect to the corresponding predictions. With the exception of JW 660, all stars in the B0.5-B3 range fall in the “W” category according to their X-ray luminosity. However, a MA companion is suggested for θ^2 Ori B. Here the $\log(L_x/L_{bol})$ level is compatible with the prediction for wind-shock emission, but in absolute terms L_x is low enough to originate from a late-type T Tauri star.

JW 660 (B3) is one of three stars showing evidence for rotational modulation in the COUP. The time-evolution of its hardness ratio shows a correlation with the X-ray brightness, opposite to the *anticorrelation* found in θ^1 Ori C where the MCWS mechanism appears to dominate. Rotational modulation of the X-ray emission can result from the eclipse of a large magnetic loop by the star (Stelzer et al. 1999), and the joint modulation of intensity and temperature is typical for magnetic activity phenomena. However, we can not exclude applying the MCWS scenario to JW 660, as this model does not make predictions on the variation of hardness with phase. It would be very valuable to search JW 660 for a large-scale

magnetic field.

The remaining stars (B0-07) are the most massive in the ONC. They are all very luminous with $\log L_{t,c} > 32 \text{ erg s}^{-1}$, about one order of magnitude or more above the value “predicted” for small-scale wind shocks. Next we discuss these stars in turn.

The most extreme case is obviously θ^1 Ori C with $\log L_{t,c} \sim 33.3 \text{ erg s}^{-1}$. *ROSAT* discovered an X-ray modulation with the same period as the optical period ($P = 15.4\text{d}$; Gagné et al. 1997). To explain its extreme X-ray luminosity and rotational modulation, Babel & Montmerle (1997b) applied a MCWS model originally devised for the X-ray emission of the Ap star IQ Aur (Babel & Montmerle 1997a). For θ^1 Ori C, the MCWS model postulates a magnetic field of order 400 G buried in the wind and confining its dense, low-velocity layers. Because the outer layers of the wind were predicted to be open and sitting above the magnetically confined layers, such a magnetic field was difficult to detect. However, this was achieved by Donati et al. (2002) who found the predicted field via a rotationally modulated Zeeman effect. The COUP data enables for the first time a continuous study of X-ray spectral changes along the rotation cycle of θ^1 Ori C. The anti-correlation between source luminosity and hardness is unusual and detailed modelling is needed. At present, we speculate that the explanation for this anti-correlation results from particular viewing angles of the X-ray absorbing ‘cooling disk’ predicted by the MCWS model. In a recent study based on high-resolution spectroscopic X-ray observations of θ^1 Ori C Gagné et al. (2005) reported a small increase of the column density during phases when the disk is viewed edge-on, corresponding to the X-ray minimum. This is consistent with the increase in spectral hardness we observed during the COUP.

The second-most hot star, θ^2 Ori A (O9.5), can be accommodated in the class of small-scale wind shock emitters according to its characteristics shown during the COUP, but dramatic flares were seen in the earlier *Chandra* observation described by Feigelson et al. (2002). These flares can be caused by magnetic reconnection in the wind (which implies that this star be magnetic), or by an unusually active unseen MA companion.

θ^1 Ori A similarly shows hybrid characteristics. This star shows evidence for magnetic fields from its non-thermal radio emission (Felli et al. 1993), and an X-ray spectroscopic study shows plasma with temperatures up to 43 MK (Schulz et al. 2003). With its flare-like behavior, it reaches X-ray luminosities unusually high for a low-mass MA companion. We speculate that its magnetic field is too weak for the wind to be confined, but that strong reconnection events take place along the wind. If the star rotates, the wind flow will, like the solar wind, take the shape of an Archimedean spiral past the Alfvén radius. In such a configuration, “corotating interaction regions” (CIRs) analogous to those in the solar wind (e.g., Kissmann et al. 2004), or in the wind of the young pole-on B star AB Aur (Catala

et al. 1999), may exist. These CIRs could trigger reconnection events, such as proposed by Usov & Melrose (1992), to which the flare-like events observed on θ^1 Ori A by COUP might be related. A direct search for magnetic fields on the stellar surface would be valuable. We recall, however, that θ^1 Ori A has two known lower-mass companions, and possibly others still undetected. The observed X-rays could arise from one extraordinarily MA companion, similar perhaps to LkH α 312 seen elsewhere in the Orion molecular cloud (Grosso et al. 2004).

8. Conclusions

The COUP observation has permitted an in-depth study of the X-ray emission of the early-type stars of the ONC with the unprecedented exposure covering most of 13.2 contiguous days. We examine a sample of 20 coeval O, B and A stars. We address the X-ray properties and underlying astrophysical processes of two subclasses: 9 hotter members with spectral types O7–B3, designated ‘strong wind’ or SW stars, and 11 cooler members with spectral types B5–A9, designated ‘weak wind’ or WW stars. We also investigate the effects of multiplicity, disks, and independent evidence for stellar magnetic fields.

Addressing the mystery of X-ray emission from intermediate-mass late-B and A stars, we find an extraordinary range in luminosities ranging from nondetections with $\log L_X < 27.6$ erg s $^{-1}$ comparable to the quiet Sun to violently flaring sources up to $\log L_X \simeq 31$ erg s $^{-1}$. Based on flaring lightcurves and hard spectra, the detected WW stars are very likely associated with unseen late-type companions. The case of θ^1 Ori E (B5) is unusual with strong constant X-ray luminosity around $L_X \simeq 2 \times 10^{32}$ erg s $^{-1}$ and flares of comparable intensity. Exhibiting non-thermal radio emission, this may be a case for MCWS emission in a mid-B star.

The situation with the Trapezium SW OB stars is rich and intriguing. The X-ray emission gives little support for the long-standing claim that L_x/L_{bol} is constant around $\simeq 10^{-7}$ for OB stars. While a rough trend between L_x and L_{bol} is seen, three orders of magnitude scatter in L_x can be present at a given L_{bol} ³. We note that this result is limited by the Orion population to stars of spectral type O7 and later, and we can not say whether a constant L_x/L_{bol} is present for the most luminous early-O stars.

The X-ray properties from the majority of the SW stars exhibit hybrid characteristics.

³We suggest that the previous evidence, particularly the *ROSAT* All-Sky Survey of OB stars (Berghöfer et al. 1997), suffered a distance-related selection bias and missed the lower luminosity stars.

Only θ^1 Ori D (B0.5) and NU Ori (B1), and perhaps the faint Par 1772 (B2) and θ^1 Ori B East (B3), exclusively show the roughly constant, soft spectrum emission attributable to the traditional Lucy-White model of small-scale wind shocks. Most show combinations of soft wind emission, hard-spectrum short-lived flares, and/or rotational modulation. If the flares of θ^2 Ori A from a previous *Chandra* observation are included, all three of the hottest Trapezium stars – θ^1 Ori C (O7), θ^2 Ori A (O9.5) and θ^1 Ori A (B0) – show these hybrid characteristics. Together with independent indicators of magnetic fields, the COUP evidence strongly supports the MCWS model where the harder and variable X-rays are produced by magnetically-mediated large-scale shocks.

The eleven cooler WW stars lack both strong ultraviolet emission to drive powerful winds and outer convection zones to drive a solar-like dynamo. They are thus predicted to be X-ray-quiet. Yet seven of these stars are detected in the COUP image and together they exhibit a wide range of X-ray luminosities from $\log L_x < 27.6 \text{ erg s}^{-1}$ comparable to the contemporary Sun to flares up to $\log L_x \sim 31 \text{ erg s}^{-1}$. Based on their flaring lightcurves and hard spectra, very similar to COUP properties of lower-mass stars in the ONC, we believe that the WW X-ray emission is most likely produced by late-type companions. In one case, θ^1 Ori B, the high-multiplicity system is resolved into two X-ray sources; one component seems to be a soft-spectrum wind source and the other one a flaring MA lower-mass companion. The COUP study uncovered a similar multiple system, heavily obscured by the Orion Molecular Cloud: the hot Becklin-Neugebauer Object has a faint X-ray source that is nearly overwhelmed by a much brighter, previously unknown low-mass companion (Grosso et al. 2005).

Our boundary at spectral type B4 between SW and WW stars is probably not a strict divide between wind and companion X-ray emission in all stars. The case of θ^1 Ori E at B5 is unusual, showing strong constant X-ray emission around $L_x \sim 2 \cdot 10^{32} \text{ erg s}^{-1}$ and flares of comparable intensity. It may represent a case for MCWS emission in a mid-B star.

We emerge from the present study with an increasing recognition of the important role played by magnetic fields in massive stellar systems. In many cases, the X-ray properties no longer follow the simple ideas of small-scale shocks from unstable radiatively accelerated winds. Violent reconnection events, either in the winds of the massive primary or from MA orbiting late-type companions, are frequently present. Rotational modulation of the X-ray signal is not infrequent. The high fraction of OB stars which are suggested from X-ray emission to have magnetically confined winds is much higher than the few percent of B stars possessing optically detected magnetic surfaces (Landstreet 2003). X-rays thus provide a powerful diagnostic for OB magnetospheres and their interactions with radiatively accelerated winds. The evidence provided here concerning the prevalence of strong magnetic fields in the hotter O7–B0 stars, where optical detection techniques are difficult, may be

particularly important.

It is now necessary to search for unresolved late-type companions down to distances ~ 10 AU, as is currently possible with high-angular resolution optical and IR methods. On the other hand, our study must encourage renewed efforts to search for magnetic fields in OB stars, in particular in the Orion Trapezium.

A. Multiple stellar systems

Here we present observational information on individual multiple systems in order of decreasing spectral type of the primary component.

A.1. θ^1 Ori C – COUP 809

θ^1 Ori C is a speckle binary with $0.037''$ separation (or 16 AU projected linear separation), composed of the $45 M_{\odot}$ primary and a $> 6 M_{\odot}$ secondary (Schertl et al. 2003). It is the most massive star in the Trapezium cluster, and also extraordinary in terms of its X-ray properties: highest X-ray luminosity among the COUP sources ($\log L_{t,c} [\text{erg/s}] \sim 33.3$), rotational modulation of the X-ray emission in accordance with the optical variations, hardness anti-correlated with the lightcurve along the 15.4 d cycle. These peculiarities make it likely that the X-ray emission originates on the O star.

Although we took carefully care of correcting for pile-up effects, the extracted spectrum of this extremely X-ray luminous source may still be affected by pile-up, so that the spectral parameters and the luminosity are possibly misestimated. Schulz et al. (2001) derived $\log L_x [\text{erg s}^{-1}] \simeq 32.3$ from the zeroth order signal of an ACIS/HETG observation. But Gagné et al. (2005) found $\log L_x [\text{erg s}^{-1}] \simeq 33$ from the same data set, in rough agreement with the COUP result. Furthermore, Flaccomio et al. (2003) found $\log L_x [\text{erg s}^{-1}] \simeq 33.2$, consistent with our COUP result, from a *Chandra* HRC observation, which is free of pile-up effects.

A.2. θ^2 Ori A – COUP 1232

This system is a hierarchical triple with a $25 M_{\odot}$ O9.5 primary (Preibisch et al. 1999), a $\simeq 9 M_{\odot}$ A2 spectroscopic companion (Aikman et al. 1974; Abt et al. 1991; Morrell & Levato 1991) and a $\simeq 7 M_{\odot}$ visual companion with separation $0.38''$ (Mason et al. 1998;

Preibisch et al. 1999). The X-ray emission is unusually strong $\log L_{t,c} = 32.5 \text{ erg s}^{-1}$ after correction for absorption. The COUP source suffers heavy pileup and only 1% of the events are extracted for analysis.

Such high levels of activity are rarely seen in lower mass T Tauri stars and, in such cases, are always associated with high amplitude ($L_{\text{flare}}/L_{\text{char}} \gg 10$), hard spectrum ($kT \simeq 5 - 8 \text{ keV}$) flares (e.g., Tsuboi et al. 1998; Grosso et al. 2004; Feigelson et al. 2005; Favata et al. 2005). However, $\theta^2 \text{ Ori A}$ is only weakly variable over the 13-day COUP observation: no flare is seen and the luminosity ratio between the highest segment and the characteristic level is $L_{\text{peak}}/L_{\text{char}} = 1.8$. In the earlier *Chandra* ACIS study of the ONC of Feigelson et al. (2002), $\theta^2 \text{ Ori A}$ exhibited multiple flares with peak $\log L_t \simeq 31.8 \text{ erg s}^{-1}$ superposed on a relatively constant component. This was the most dramatic variation then known from an OB stellar system and can be attributed either to rapidly changing large-scale shocks in a magnetically confined stellar wind of the massive primary, or to unusually powerful magnetic reconnection flares in a lower mass companion.

The spectrum is well-fit by a two-temperature plasma dominated by the soft component. The absorption column derived from the X-ray spectrum is compatible with the optical extinction. We thus believe the emission arises from the massive primary wind and not a MA secondary. Note that our individually constructed X-ray spectral fit differs from that obtained by Getman et al. (2005a) from a semi-automated procedure. They reported a much lower absorbing column density, and hence lower value of the absorption-corrected $\log L_{t,c}$.

A.3. $\theta^1 \text{ Ori A} - \text{COUP 745}$

$\theta^1 \text{ Ori A}$ is at least a triple system with a $16 M_{\odot}$ B0.5 primary (Schertl et al. 2003). The nearer companion has an eclipsing 65 day orbit; models of the optical lightcurve suggests a pre-main sequence $\sim 3 M_{\odot} \sim \text{A0}$ star (Lloyd & Strickland 1999). The distant companion is a $4 M_{\odot}$ late-B star with $0.2''$ separation (Petr et al. 1998; Weigelt et al. 1999; Preibisch et al. 1999). The system is a highly variable radio source with spectral and polarization properties characteristic of non-thermal flaring (Felli et al. 1993).

$\theta^1 \text{ Ori A}$ is a strong X-ray source which is affected by photon pile-up in the ACIS detector. During the 13-day COUP observation, it exhibited a nearly-constant ‘characteristic’ level of $\log L_{t,c} \simeq 32.4 \text{ erg s}^{-1}$ superposed with several flares with peak luminosities around $31.9 - 32.6 \text{ erg s}^{-1}$. A range of plasmas with energies from 0.7 to $>2 \text{ keV}$ are present.

A.4. NU Ori – COUP 1468

NU Ori is at least a hierarchical triple binary with a $14 M_{\odot}$ B1 primary, a $\simeq 3 M_{\odot}$ spectroscopic companion with period of 8 days (Morrell & Levato 1991), and a $\simeq 1 M_{\odot}$ companion with separation $0.47''$ (Preibisch et al. 1999). The COUP X-ray luminosity is $\log L_{t,c} = 31.2 \text{ erg s}^{-1}$. This source was located $8'$ off-axis where the *Chandra* point spread function is degraded, so the $0.4''$ offset between the COUP and primary component positions can be reconciled with emission from any of the components. However, the L_x/L_{bol} level is that of a typical wind X-ray source, and NU Ori showed no sign of variability during the 13-day observation. Together, these characteristics suggest that the observed emission comes from the primary and can be explained within the standard scenario of stellar winds.

A.5. θ^1 Ori B – COUP 766+778

This system is at least a quintet. Near-IR images of the system are provided by Simon et al. (1999) and by Schertl et al. (2003). The brightest member is the B2.5 component θ^1 Ori B East with mass $6.3 M_{\odot}$ (Prato et al. 2002). It is an eclipsing binary (hence the variable star designation BM Ori). The secondary is a rapidly rotating pre-main sequence star with large IR excess, estimated spectral type of G2 (Popper & Pavc 1976; Antokhina et al. 1989; Vitrichenko & Plachinda 2000), and mass of $\sim 2.7 M_{\odot}$ (Palla & Stahler 2001). θ^1 Ori B West lies $0.94''$ to the southwest and is a resolved binary with $0.14''$ separation. The estimates for the masses of these two components range between $4 - 1.6 M_{\odot}$ and $3 - 0.7 M_{\odot}$, respectively (Schertl et al. 2003; Preibisch et al. 1999). The faintest known member of the quintet has *K*-band magnitude 10.5 (Simon et al. 1999) with estimated mass $0.2 M_{\odot}$ (Preibisch et al. 1999), and lies $\sim 0.6''$ northwest of θ^1 Ori B East.

θ^1 Ori B is the only visual multiple that is resolved into multiple COUP sources, although several dozen COUP doubles with separations $< 3''$ are seen in the MA population (Getman et al. 2005b). The COUP image of the region, shown in Figure 8, shows two X-ray sources: θ^1 Ori B East (COUP 778) and West (COUP 766). About 1/3 of the events from each source is retrieved with the *ACIS Extract* procedure to reduce cross-contamination of the point spread functions. However, some residual contamination of the luminous flare in the brighter source 766 is seen in the lightcurve of the weaker source 778 (Figure 5).

θ^1 Ori B East (COUP 778) with $\log L_{t,c} = 30.1 \text{ erg s}^{-1}$ has an unusually soft spectrum without strong variability. The emission is thus plausibly attributed to wind shocks of the B2.5 primary, rather than to reconnection flares in its G2-type companion.

In contrast, θ^1 Ori B West (COUP 766) has all the characteristics of a magnetically active

lower-mass member of the Orion population (Wolk et al. 2005; Favata et al. 2005). It shows several flares including a very powerful one exhibiting rapid rise with a hard spectrum, peak luminosity around $\log L_t \simeq 31.5 \text{ erg s}^{-1}$, and slower decay over several hours with a softening spectrum. It is not clear which of the components of the θ^1 Ori B West binary is the principal X-ray emitter.

B. New X-ray Detection of Par 1772 (= COUP 349)

The high spatial resolution of *Chandra* combined with the high sensitivity achieved during the extraordinary long exposure of the COUP has brought forth a new X-ray detected B1.5 star, Par 1772. It is sometimes considered a Herbig Be star due to mid-IR excess in the *IRAS* satellite data and optical reddening. However, it does not exhibit emission lines indicating accretion nor near-IR photometric excess emission indicating a warm inner disk, as seen in other Herbig Be stars (Manoj et al. 2002). It may have an annular disk. No companions were seen in speckle imaging (Preibisch et al. 1999).

In X-rays, the star was reported at a level of $\log L_s \simeq 30.2 \text{ erg s}^{-1}$ from *ROSAT* HRI observations in 1991-92 (Caillault et al. 1994). However, the offset was reported to be $7''$ so it seems likely that the association was confused by the three COUP sources within $\simeq 10''$ (see Fig. 10). The star was not detected in 1999-2000 *Chandra* ACIS or HRC observations (Feigelson et al. 2002; Flaccomio et al. 2003). During the COUP 2003 exposure, it appeared as a weak and roughly constant source with $\log L_{t,c} = 28.9 \text{ erg}^{-1}$. Together with θ^2 Ori B, it has one of the lowest $\log(L_x/L_{\text{bol}})$ values ($= -7.9$) ever seen in a stellar X-ray source. We can not determine whether the emission arises from the massive primary or an unseen companion.

We thank N. Schulz for valuable comments on the manuscript. We appreciate helpful suggestions of the referee M. Gagné. COUP is supported by *Chandra* Guest Observer grand SAO GO3-4009A (E. Feigelson, PI). B.S., E.F., G.M. and S.S. acknowledge financial support from the Italian MIUR FRIN program and an INAF program for the years 2002-04. E.D.F. received support from the *Chandra* ACIS Team contract NAS8-38252.

REFERENCES

- Abbott D. C., 1979, in Mass loss and evolution of O-type stars, P. S. Conti & C. de Loore (eds.), IAU Symp. 83, Dordrecht: Reidel, p.237
- Abbott D. C., Bieging J. H. & Churchwell E., 1984, ApJ 280, 671
- Abt H. A., Wang R. & Cardona O., 1991, ApJ 367, 155
- Aikman G. C. L. & Goldberg B. A., 1974, J. Roy. Astron. Soc. Canada, 68, 205
- Anders E. & Grevesse N., 1989, Geochim. Cosmochim. Acta 53, 197
- Antokhina E. A., Ismailov N. Z. & Cherpashchuk A. M., 1989, Sov.A.L. 15, 362
- Babel J., 1996, A&A 309, 867
- Babel J. & Montmerle T., 1997a, A&A 323, 121
- Babel J. & Montmerle T., 1997b, ApJ 485, L29
- Berghöfer T. W., Schmitt J. H. M. M., Danner R. & Cassinelli J. P., 1996, A&A 322, 167
- Behar, E., Leutenegger, M., Doron, R., Güdel, M., Feldman, U., Audard, M., & Kahn, S. M. 2004, ApJ, 612, L65
- Bernabeu G., Magazzú A. & Stalio R., 1989, A&A 226, 215
- Bessel M. S. & Brett J. M., 1988, PASP 100, 1134
- Böhm T. & Catala C., 1995, A&A 301, 155
- Bouvier J., Chelli A., Allain S., et al., 1999, A&A 349, 619
- Caillault J.-P., Gagné M. & Stauffer J. R., 1994, ApJ 432, 386
- Caillault J.-P. & Zoonematkermani S., 1989, ApJ 338, L57
- Carpenter J. M., Hillenbrand, L. A. & Skrutskie M. F., 2001, AJ 121, 3160
- Castor J., Abbott D. & Klein R., 1975, ApJ 195, 157
- Catala C., Donati J. F., Böhm, T., et al., 1999, A&A 345, 884
- Charbonneau P. & MacGregor K. B., 2001, ApJ 559, 1094
- Choi P. I. & Herbst W., 1996, AJ 111, 283

- Cohen D. H., Cassinelli J. P. & Macfarlane J. J., 1997, *ApJ* 487, 867
- Cohen, D. H.; de Messières, G. E.; MacFarlane, J. J.; Miller, N. A.; Cassinelli, J. P.; et al., 2003, *ApJ* 586, 495
- Corporon P. & Lagrange A.-M., 1999, *A&AS* 136, 429
- de Jong J. A., Henrichs A. F., Kaper L., et al., 2001, *A&A* 368, 601
- Donati J.-F., Babel J., Harries T. J., et al., 2002, *MNRAS* 333, 55
- Favata F., Flaccomio, E., et al. 2005, *ApJS*, in press
- Favata F. & Micela M., 2003, *Space Science Reviews* 108, 577
- Feigelson, E. D., Getman, K. V., et al., *ApJS*, in press
- Feigelson E. D., Lawson W. A. & Garmire G. P., 2003, *ApJ* 599, 1207
- Feigelson E. D., Broos P., Gaffney J. A. III., et al., 2002, *ApJ* 574, 258
- Feigelson E. D. & Montmerle T., 1999, *ARA&A* 37, 363
- Feigelson E. D. & Nelson P. I., 1985, *ApJ* 293, 192
- Felli M., Taylor G. B., Catarzi M., Churchwell E. & Kurtz S., 1993, *A&AS* 101, 127
- Flaccomio E., Damiani F., Micela G., et al., 2002, *ApJ* 582, 382
- Flaccomio E., et al., 2005, *ApJS*, in press
- Frost E. B., Barrett S. B. & Struve O., 1926, *ApJ* 64, 1
- Gagné M., Oksala M. E., Cohen D. H., Tonnesen S. K., Ud-Doula A., et al., 2005, *astro-ph/0504296*
- Gagné M., Caillault J.-P., Stauffer J. R. & Linsky J. L., 1997, *ApJ* 478, L87
- Getman K., Flaccomio E., Broos P., et al., 2005a, *ApJ* in press
- Getman K., et al., 2005b, *ApJS*, in press
- Grosso N., Feigelson, E. D., et al., 2005, *ApJS*, in press
- Grosso N., Montmerle T., Feigelson E. D. & Forbes T. G., 2004, *A&A* 419, 653
- Hamaguchi K., Yamauchi S. & Koyama K., 2005, *ApJ* 618, 360

- Harnden F. R. Jr., Branduardi G., Gorenstein P., Grindlay J., Rosner R., et al., 1979, ApJ 234, 51
- Herbst W., Rhode K.L., Hillenbrand L.A. & Curran G., 2000, AJ 119, 261
- Hillenbrand L. A. & White R. J., 2004, ApJ 604, 741
- Hillenbrand L. A., Strom S. E., Calvet N., et al., 1998, AJ 116, 1816
- Hillenbrand L. A., 1997, AJ 113, 1733
- Kaper L., Henrichs H. F., Nichols J. S. & Telting J. H., 1999, A&A 344, 231
- Kissmann R., Fichtner H. & Ferreira S. E. S., 2004, A&A 419, 357
- Kudritzki R.-P. & Puls J., 2000, ARA&A 38, 613
- Landstreet J. D., 2003, In: Proc. of ‘Magnetism and Activity of the Sun and Stars’, EAS Publications Series, vol. 9, 235
- Landstreet J. D., 1992, A&AR 4, 35
- Linsky J. L., Drake S. A. & Bastian T. S., 1992, ApJ 393, 341
- Lloyd C. & Strickland D. J., 1999, IBVS 4809
- Lucy L. B. & White R. L. 1980, ApJ 241, 300
- MacGregor K. B. & Cassinelli J. P., 2003, ApJ 586, 480
- Manoj P., Maheswar G. & Bhatt H. C., 2002, MNRAS 334, 419
- Mason B. D., Gies D. R., Hartkopf W. I., et al., 1998, AJ 115, 821
- Mewe R., Gronenschild E. H. B. M. & van den Oord G. H. J., 1985, A&AS 62, 197
- Mewe R., Kaastra J., S., Schrijver C. J., van den Oord G. H. J. & Alkemade F. J. M., 1995, A&A 296, 477
- Miller N. A., Cassinelli J. P., Waldron W. L., MacFarlane J. J. & Cohen D. H., 2002, ApJ 577, 951
- Montmerle Th., Grosso N., Tsuboi Y. & Koyama K., 2000, ApJ 532, 1097
- Montmerle Th., Koch-Miramond L., Falgarone E. & Grindlay J. E., 1983, ApJ 269, 182

- Morrell N. & Levato H., 1991, *ApJS* 75, 965
- Münch A. A., Lada E. A., Lada C. J. & Alves Joao, 2002, *ApJ* 573, 366
- Nakajima H., Imanishi K., Takagi S.-I., Koyama K. & Tsujimoto M., 2002, *PASJ* 55, 635
- Oksala, M., Gagne, M., Cohen, D., Tonnesen, S., ud-Doula, A., Owocki, S., & MacFarlane, J. 2004, *Bull. AAS*, 204, #62.14
- Owocki S. P. & Cohen D. H., 1999, *ApJ* 520, 833
- Palla F. & Stahler S. W., 2001, *ApJ* 553, 299
- Pallavicini R., Golub L., Rosner R., Vaiana G. S., Ayres T., et al., 1981, *ApJ* 248, 279
- Petr M. G., Coudé du Foresto V., Beckwith S. V. W., et al., 1998, *ApJ* 500, 825
- Popper D. M. & Plavec M., 1976, *ApJ* 205, 462
- Prato L., Simon M., Mazeh T., et al., 2002, *ApJ* 569, 863
- Preibisch Th., et al., 2005, *ApJS*, in press
- Preibisch Th., 2003, *A&A* 401, 543
- Preibisch Th. & Zinnecker H., 2001, *AJ* 123, 1613
- Preibisch Th., Balega Y., Hofmann K.-H., Weigelt G. & Zinnecker H., 1999, *New Astronomy* 4, 531
- Preibisch Th., 1997, *A&A* 320, 525
- Renson P., Gerbaldi M. & Catalano F. A., 1991, *A&AS* 89, 429
- Rieke G. H. & Lebofsky M. J., 1985, *ApJ* 288, 618 (RL85)
- Scargle J. D., 1982, *ApJ* 263, 835
- Scargle J. D., 1998, *ApJ* 504, 405
- Schertl D., Balega Y. Y., Preibisch Th. & Weigelt G., 2003, *A&A* 402, 267
- Sciortino S., Vaiana G. S., Harnden F. R. Jr., Ramella M., Morossi C., et al., 1990, *ApJ* 361, 621

- Schmitt J. H. M. M., Golub L., Harnden F. R. Jr., Maxson C. W., Rosner R., et al., 1985, ApJ 290, 307
- Schulz N. S. Canizares C., Huenemoerder D., et al., 2001, ApJ 549, 441
- Schulz, N. S., Canizares, C., Huenemoerder, D., & Tibbets, K. 2003, ApJ, 595, 365
- Siess L., Dufour E. & Forestini M., 2000, A&A 358, 598
- Simon M., Close L. M. & Beck T. L., 1999, AJ 117, 1375
- Simon Th., Drake S. A. & Kim P. D., 1995, PASP 107, 1034
- Smith, M. A., & Fullerton, A. W. 2005, PASP, 117, 13
- Snow Th. P. & Morton D. C., 1976, ApJ 32, 429
- Stahl O., Kaufer A., Rivinius Th., et al., 1996, A&A 312, 539
- Stahl O., Wolf B., Gäng Th., et al., 1993, A&A 274, L29
- Stelzer B., Huélamo,N., Hubrig S., Micela G., Zinnecker H. & Guenther E., 2005, in 13th Cambridge Workshop on Cool Stars, Stellar Systems, and the Sun, ESA SP Ser., in press
- Stelzer B., Huélamo,N., Hubrig S., Zinnecker H. & Micela G., 2003, A&A 407, 1067
- Stelzer B., Neuhäuser R., Casanova S & Montmerle T., 1999, A&A 344, 154
- Thé P. S., de Winter D. & Perez M. R., 1994, A&AS 104, 315
- Tsuboi Y., Koyama K. & Murakami H., 1998, ApJ 503, 894
- Tovmassian H. M., Navarro S. G., Tovmassian G. H., et al., 1997, AJ 113, 1888
- Trigilio C., Leto P., Umana G., Leone F. & Buemi C. S., 2004, A&A 418, 593
- Ud'Doula A. & Owocki S. P., 2002, ApJ 576, 413
- Usov V. V. & Melrose D. B., 1992, ApJ 395, 575
- van Loo S., Runacres M. C. & Blomme R., 2004, A&A 418, 717
- Vitrichenko E. A. & Plachinda S. I., 2000, AstL 26, 390
- Vuong M. H., Montmerle T., Grosso N., et al., 2003, A&A 408, 581

Weigelt G., Balega Y., Preibisch Th., et al., 1999, A&A 347, L15

Wolk S. J., et al., 2005, ApJS, in press

Table 1. Stellar parameters of early-type stars in the COUP field of the ONC

ID	V mag	A_V mag	SpTy	$\log T_{\text{eff}}$ K	$\log L_{\text{bol}}$ L_{\odot}	Multiplicity			
						SB? ^a	VB? ^b	Optical? ^c	Disk? ^d
‘Strong-Wind’ Sample									
θ^1 Ori C	5.140	1.74	O7	4.603	5.40	–	×
θ^2 Ori A	5.070	1.12	O9.5	4.543	5.03	×	×
θ^1 Ori A	6.730	1.89	B0	4.471	4.50	×	×
θ^1 Ori D	6.700	1.79	B0.5	4.420	4.35	–	–
NU Ori	6.840	2.09	B1	4.383	4.33	×	×	...	×
θ^2 Ori B	6.410	0.73	B1	4.383	3.96	–	–
Par 1772	8.370	1.47	B2	4.294	3.27	...	–	...	×
JW 660	9.620	2.44	B3	4.272	3.11
θ^1 Ori B	7.260	0.49	B3	4.272	3.28	...	×	×	?
‘Weak-Wind’ Sample									
θ^2 Ori C	8.240	0.92	B5	4.140	2.79	?	×
θ^1 Ori E	–	–	B5	4.140	2.42
θ^1 Ori F	–	–	B8	4.053	1.84	...	–
JW 197	10.16	0.85	B9	4.025	1.69	–
JW 153	8.920	0.13	B9	4.025	1.89	–	×
JW 831	9.470	0.00	A0	3.993	1.54	–
JW 531	10.55	1.56	A1	3.975	1.71	×
JW 108	10.19	2.07	A3	3.940	2.01	–	?
JW 608	11.89	1.29	A5	3.917	1.00
JW 165	13.55	4.20	A7	3.897	1.49
JW 599	19.20	10.7	A9	3.867	1.86	?

^aCrosses indicate variable radial velocity or confirmed spectroscopic binary, dashes indicate constant radial velocity (Frost et al. 1926; Abt et al. 1991; Morrell & Levato 1991).

^bCrosses indicate visual companions identified in speckle surveys (Weigelt et al. 1999; Preibisch et al. 1999; Petr et al. 1998; Simon et al. 1999; Mason et al. 1998), dashes indicate negative results.

^cOptical binaries identified by eclipses are indicated by crosses (Antokhina et al.

1989).

^dCrosses mark HAeBe candidates (Thé et al. 1994; Tovmassian et al. 1997). ‘?’ mark stars with *L*-band excess in the near-IR color magnitude diagram (Figure 11).

Table 2. COUP X-ray properties of early-type stars in the ONC

COUP #	ID	SpTy	Offaxis '	Δ_{ix} "	NetCts	PSF frac	Exp ks	HR	FBG02 #
‘Strong-Wind’ Sample									
809	θ^1 Ori C	O7	0.32	0.05	63444	0.01	834.7	0.26 ± 0.00	542
1232	θ^2 Ori A	O9.5	1.95	0.15	3525	0.01	827.6	0.09 ± 0.01	828
745	θ^1 Ori A	B0	0.53	0.13	21283	0.02	834.7	0.34 ± 0.01	498
869	θ^1 Ori D	B0.5	0.39	0.12	7901	0.87	832.9	0.04 ± 0.00	584
1468	NU Ori	B1	8.41	0.40	2237	0.67	728.6	0.03 ± 0.00	996
1360	θ^2 Ori B	B1	2.69	0.15	1293	0.86	767.5	0.21 ± 0.02	916
349	Par 1772	B2	4.58	0.08	127	0.87	758.6	0.18 ± 0.05	...
1116	JW 660	B3	2.13	0.07	52865	0.87	818.7	0.65 ± 0.01	746
778	θ^1 Ori BE	B3	0.60	0.13	1506	0.37	832.9	0.17 ± 0.02	519
‘Weak-Wind’ Sample									
1473	θ^2 Ori C	B5	3.92	0.17	26525	0.86	763.9	0.38 ± 0.01	995
732	θ^1 Ori E	B5	0.59	0.11	37523	0.04	834.7	0.34 ± 0.01	495
	θ^1 Ori F	B8	< 29	...	822.5
142	JW 197	B9	4.50	0.18	5311	0.87	811.7	0.29 ± 0.01	103
100	JW 153	B9	8.61	0.38	679	0.89	594.2	0.14 ± 0.02	70
1415	JW 831	A0	3.90	0.08	866	0.87	801.1	0.08 ± 0.01	952
	JW 531	A1	< 20	...	815.9
	JW 108	A3.5	< 66	...	454.9
	JW 608	A5	< 40	...	801.2
113	JW 165	A7	9.44	0.32	6724	0.89	212.2	0.32 ± 0.01	81
995	JW 599	A9	6.20	0.16	214	0.87	767.5	0.75 ± 0.13	670

Table 3. COUP X-ray spectral parameters of early-type stars in the ONC

COUP #	ID	SpTy	$\log N_{\text{H}}$ cm^{-2}	kT_1 keV	kT_2 keV	kT_3 keV	$\log EM_1$ cm^{-3}	$\log EM_2$ cm^{-3}	$\log EM_3$ cm^{-3}	χ^2_{ν} (dof)	$\log L_t$ erg s^{-1}	$\log L_{t,c}$ erg s^{-1}	$\log (L_{t,c}/L_{\text{bol}})$
‘Strong-Wind’ Sample													
809	θ^1 Ori C	O7	21.2	0.59	1.38	...	55.8	56.2	...	5.59 (219)	33.1	33.3	-5.7
1232	θ^2 Ori A	O9.5	21.5	0.23	2.45	...	55.8	54.1	...	0.83 (44)	31.8	32.5	-6.1
745	θ^1 Ori A	B0	20.9	0.66	1.68	>15	54.9	55.3	54.3	1.96 (153)	32.3	32.4	-5.7
869	θ^1 Ori D	B0.5	21.5	0.23	0.58	...	53.8	53.4	...	2.05 (61)	30.2	30.7	-7.2
1468	NU Ori	B1	21.9	0.22	>15	...	54.5	51.7	...	1.70 (25)	29.8	31.2	-6.7
1360	θ^2 Ori B	B1	21.2	0.85	2.88	...	52.4	52.3	...	1.15 (13)	29.5	29.6	-7.9
349	Par 1772	B2	21.7	0.44	2.58	...	51.9	51.2	...	1.04 (13)	28.4	28.9	-7.9
1116	JW 660	B3	21.7	0.97	3.33	...	53.8	54.3	...	1.85 (263)	31.2	31.4	-5.3
778	θ^1 Ori BE	B3	21.4	0.63	2.26	...	53.0	52.7	...	0.70 (16)	29.9	30.1	-6.7
‘Weak-Wind’ Sample													
1473	θ^2 Ori C	B5	21.4	0.86	2.86	...	53.4	53.9	...	1.88 (166)	30.9	31.0	-5.4
732	θ^1 Ori E	B5	21.1	0.64	1.58	>15	54.8	55.3	54.2	2.58 (190)	32.3	32.4	-3.6
142	JW 197	B9	21.0	0.81	3.06	...	52.6	53.0	...	1.08 (61)	30.1	30.2	-5.1
100	JW 153	B9	20.8	0.66	1.39	...	52.1	52.2	...	0.83 (29)	29.3	29.4	-6.1
1415	JW 831	A0	21.3	0.26	1.00	...	52.6	52.2	...	1.11 (31)	29.2	29.6	-5.6
113	JW 165	A7	21.4	0.87	2.41	...	53.3	53.7	...	1.54 (80)	30.7	30.9	-4.2
995	JW 599	A9	22.0	1.89	52.2	0.71 (25)	28.8	29.2	-6.3

Table 4. X-ray variability of strong-wind (SW) and weak-wind (WW) stars in the ONC

COUP #	ID	SpTy	Prob KS	Prob MLB	N_F	$\frac{t_{\text{char}}}{t_{\text{total}}}$	$\frac{R_{\text{peak}}}{R_{\text{char}}}$
‘Strong-Wind’ Sample							
809	θ^1 Ori C	O7	✓	✓	0	1.0	1.2
1232	θ^2 Ori A	O9.5	✓	✓	0	1.0	1.8
745	θ^1 Ori A	B0	✓	✓	2	0.9	2.9
869	θ^1 Ori D	B0.5	–	–	0	1.0	1.0
1468	NU Ori	B1	–	–	0	1.0	1.0
1360	θ^2 Ori B	B1	✓	✓	1	0.9	4.2
349	Par 1772	B2	✓	✓	0	1.0	1.4
1116	JW 660	B3	✓	✓	0	0.9	1.5
778	θ^1 Ori BE	B3	–	✓	1	1.0	3.3
‘Weak-Wind’ Sample							
1473	θ^2 Ori C	B5	✓	✓	3	0.7	3.0
732	θ^1 Ori E	B5	✓	✓	1	0.9	1.9
142	JW 197	B9	✓	✓	4	0.8	51.3
100	JW 153	B9	✓	✓	2	0.9	11.8
1415	JW 831	A0	✓	✓	0	1.0	1.6
113	JW 165	A7	✓	✓	1	0.9	3.8
995	JW 599	A9	–	✓	0	1.0	1.6

Table 5. Comparison of flares on SW, WW and solar-type stars in the ONC

Parameter	Sample		
	SW+WW	WW	1 M_{\odot}
N_*	9	7	28
$N_{f,\text{total}}$	15	11	41
$N_{f,\text{spec}}$	12	9	37
Median duration (ks)	13	18	65
Median $\log L_F$ (erg s^{-1})	32.3	31.2	30.8
Median $\log E_F$ (erg)	36.2	35.4	35.5

Note. — Numbers for 1 M_{\odot} stars from Wolk et al. (2005); N_* = number of stars; $N_{f,\text{total}}$ = total number of flares; $N_{f,\text{spec}}$ = number of flares with spectral information

Table 6. Periodic variability of SW and WW stars

Name	P_{opt} d	P_X d	FAP	Median cts ks^{-1}	Ampl cts ks^{-1}
θ^1 Ori C	15.42	15.51	0.000	72.6	93.9 ± 4.2
JW 660	6.15	6.67	0.001	61.3	30.7 ± 6.6
JW 165	5.77	4.61	0.001	7.8	6.1 ± 3.8

Table 7. Multiple systems with early-type primary in the COUP field of the ONC

Name	Type	Component separation				Masses (M_{\odot})		Ref.	COUP #
		Comp	Sep (mas)	PA ($^{\circ}$)	Epoch	Pri	Sec		
θ^1 Ori C	VB	C1-C2	38 ± 2	208	2001	45	≥ 6	a	809
θ^2 Ori A	VB	A1-A2	383 ± 10	291	1997	25	~ 7	b	1232
θ^2 Ori A	SB	A1-A3	100	25	~ 9	b	
θ^1 Ori A	VB	A1-A2	215 ± 3	357	2001	16	~ 4	a	745
θ^1 Ori A	ecl	A1-A3				16	~ 3	c	
NU Ori	VB	A-B	471 ± 17	98	1997	14	~ 1	b	1468
NU Ori	SB	A-C	80	14	~ 3	b	
θ^1 Ori B	VB	B1-B2	942 ± 10	255	2001	7	$\sim 4; 1.6$	a b	778+766
θ^1 Ori B	VB	B2-B3	117 ± 4	210	2001	~ 4	$\sim 3; 0.7$	a b	
θ^1 Ori B	VB	B1-B4	609 ± 8	298	2001	7	~ 0.2	a b	
θ^1 Ori B	SB	B1-B5	30	7	~ 2.7	b d	
θ^2 Ori C	SB	C1-C2	e	1473

Note. — VB = visual binary, SB = spectroscopic binary, Comp = component, Pri = primary, Sec = secondary, PA = position angle (degrees East of North)

^aSchertl et al. (2003)

^bPreibisch et al. (1999)

^cLloyd & Strickland (1999)

^dPalla & Stahler (2001)

^eCorporon & Lagrange (1999)

Table 8. Tentative classification of early-type ONC X-ray sources

COUP #	Name	SpTy	Luminosity	Spec	Var	Disk	Magn
‘Strong-Wind’ Sample							
809	θ^1 Ori C	O7	>W	...	S	...	RM,B
1232	θ^2 Ori A	O9.5	W	W	W ^a	...	
745	θ^1 Ori A	B0	>W	...	T	...	NT
869	θ^1 Ori D	B0.5	W	W	W	...	
1468	NU Ori	B1	W	W	W	fIR	
1360	θ^2 Ori B	B1	W	...	T	...	
349	Par 1772	B2	W	fIR	CP?
1116	JW 660	B3	>W	...	S	...	RM
778	θ^1 Ori BE	B3	W	nIR	
‘Weak-Wind’ Sample							
766	θ^1 Ori BW	?	T	...	
1473	θ^2 Ori C	B5	T	...	T	fIR	
732	θ^1 Ori E	B5	T	...	T	...	NT
...	θ^1 Ori F	B8	–	–	–	...	
142	JW 197	B9	T	...	T	...	
100	JW 153	B9	T	...	T	fIR	
1415	JW 831	A0	T	
...	JW 531	A1	–	–	–	fIR	
...	JW 108	A3	–	–	–	nIR	
...	JW 608	A5	–	–	–	...	
113	JW 165	A7	T	...	T/S	...	RM
995	JW 599	A9	T	nIR	

Note. — Classes: W = hydrodynamic wind (many small shocks), S = smoothly variable lightcurve, T = T Tauri type emission, nIR = near-infrared excess, fIR = far-infrared excess, RM= rotational modulation, B = detected magnetic field, CP = chemically peculiar, NT = non-thermal cm emission.

^aThis star exhibited powerful flares during the earlier *Chandra* observation described by Feigelson et al. (2002), and thus might also be classified

"T" here.

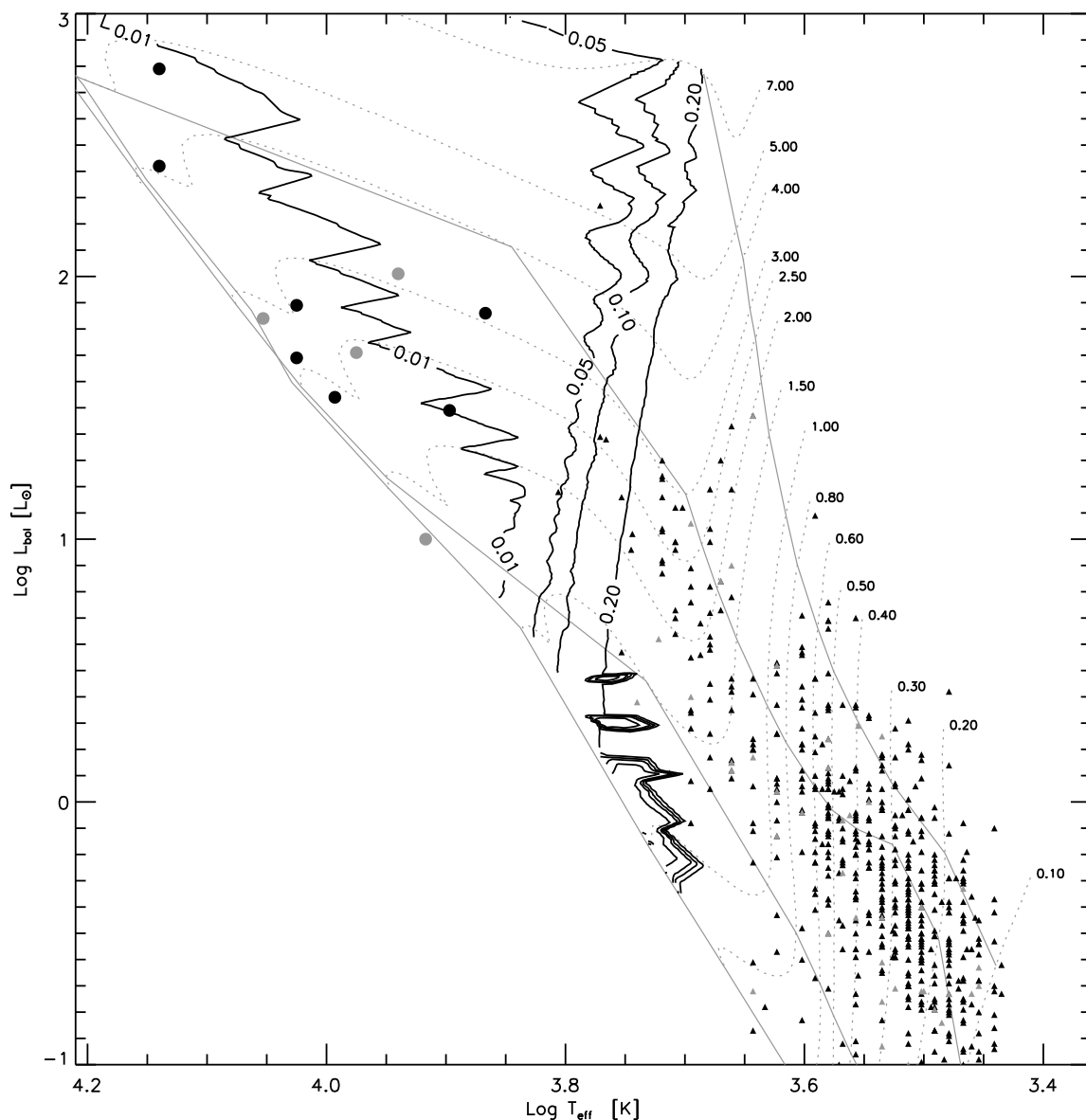


Fig. 1.— Hertzsprung-Russell diagram with pre-main sequence models from Siess et al. (2000). Dotted grey curves show isomass evolutionary tracks, solid grey curves show isochrones, and solid black jagged contours indicate the size of the convective envelopes labeled in units of the stellar radius. Symbols show spectroscopically confirmed ONC stars observed in the COUP: *triangles* are magnetically active (MA) stars, and *circles* are weak wind (WW) stars. The strong wind (SW) stars are located outside the plotted range to the left. Grey symbols indicate stars not detected in the COUP.

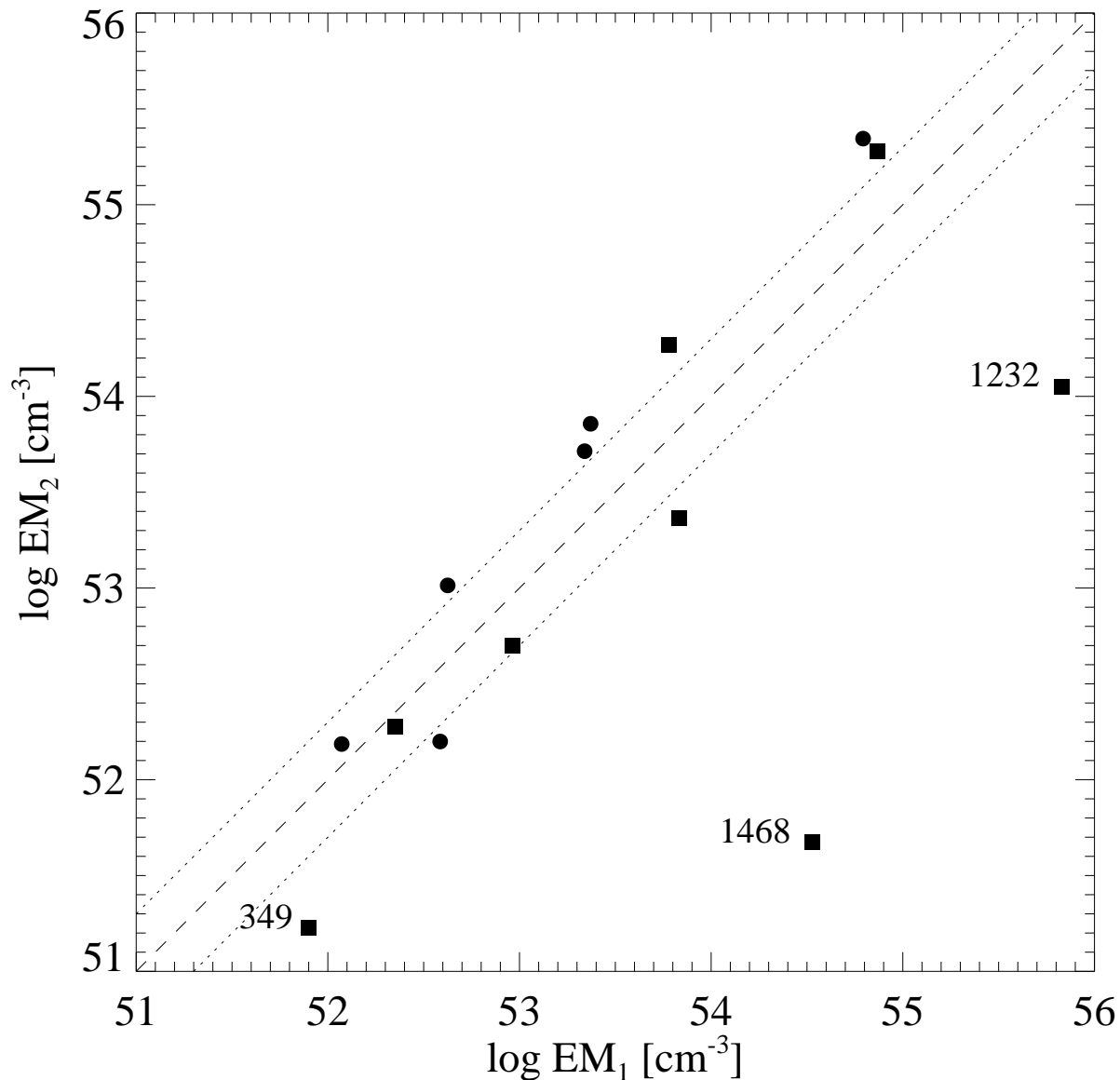


Fig. 2.— Relation between the emission measures from the two components of the spectral fits from Table 3. For 3-temperature models, we plot the EM corresponding to the two lower temperatures which dominate the emission. The region included within the dotted lines marks differences of a factor two and lower. Squares are SW stars, and circles are WW stars. Three outliers are labelled by their COUP source numbers.

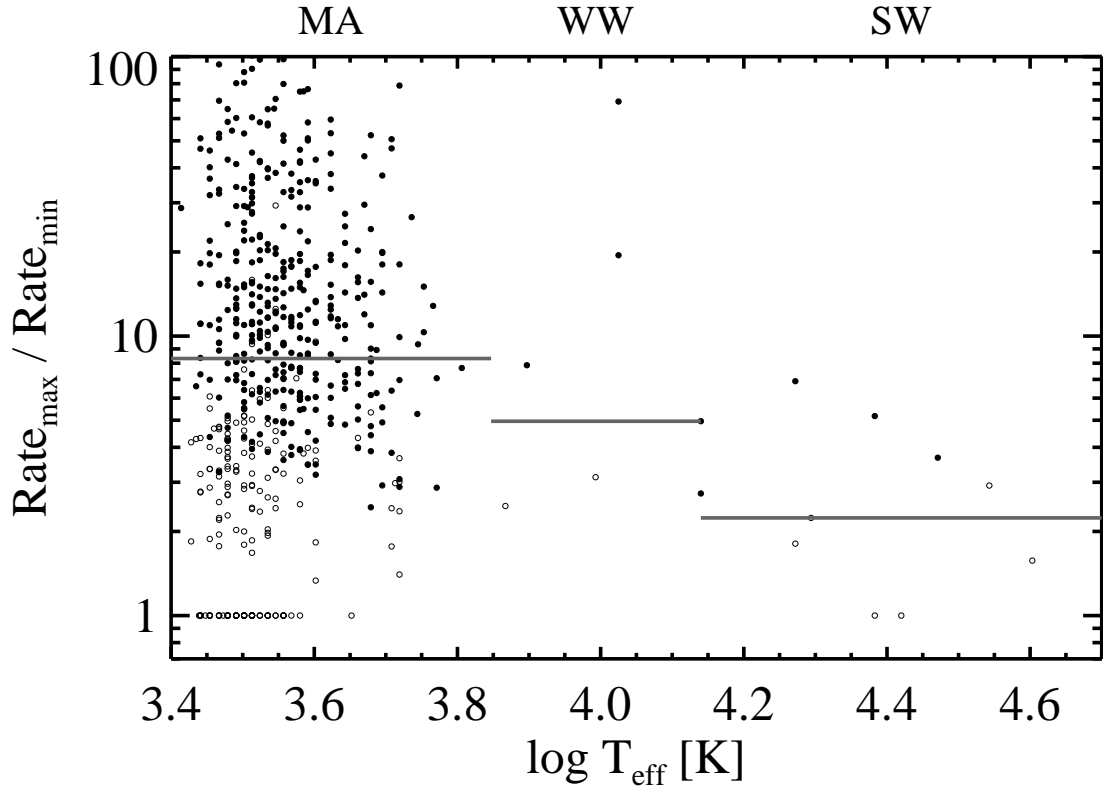


Fig. 3.— Ratio of the maximum to minimum count rate blocks in the MLB test for all sources in the COUP optical sample plotted versus the effective temperature. If the maximum count rate corresponds to a flare the plotting symbol is filled. The thick grey lines mark the median values for these ratios in each class: MA = magnetically active, WW = weak-wind, and SW = strong-wind.

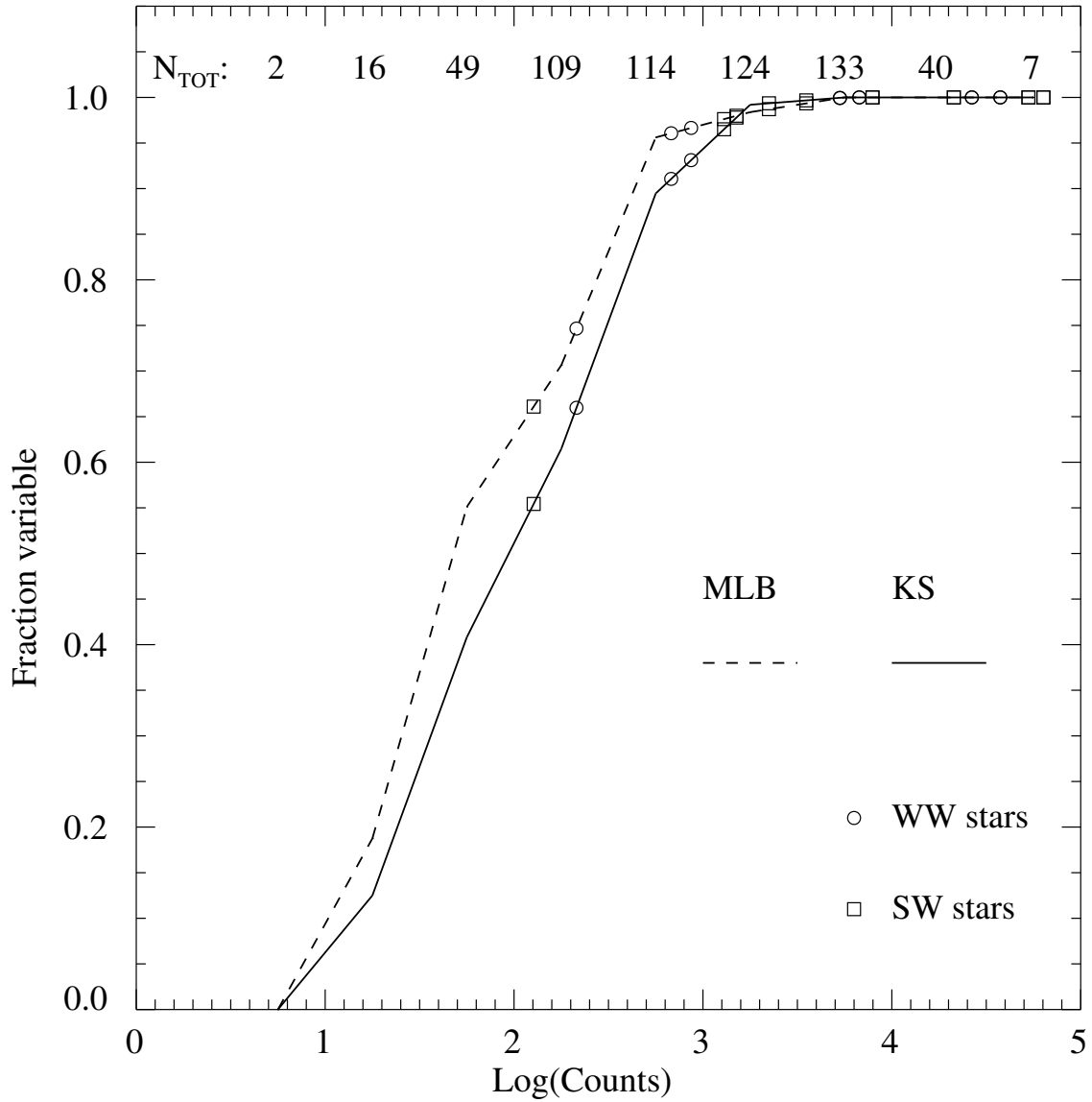


Fig. 4.— Fraction of COUP sources which are X-ray variable as a function of source brightness. The curves show the distribution for MA stars in the COUP according to Kolmogorov-Smirnov and Maximum Likelihood Blocks criteria. The individual hot SW and WW stars are plotted as open boxes and circles, respectively.

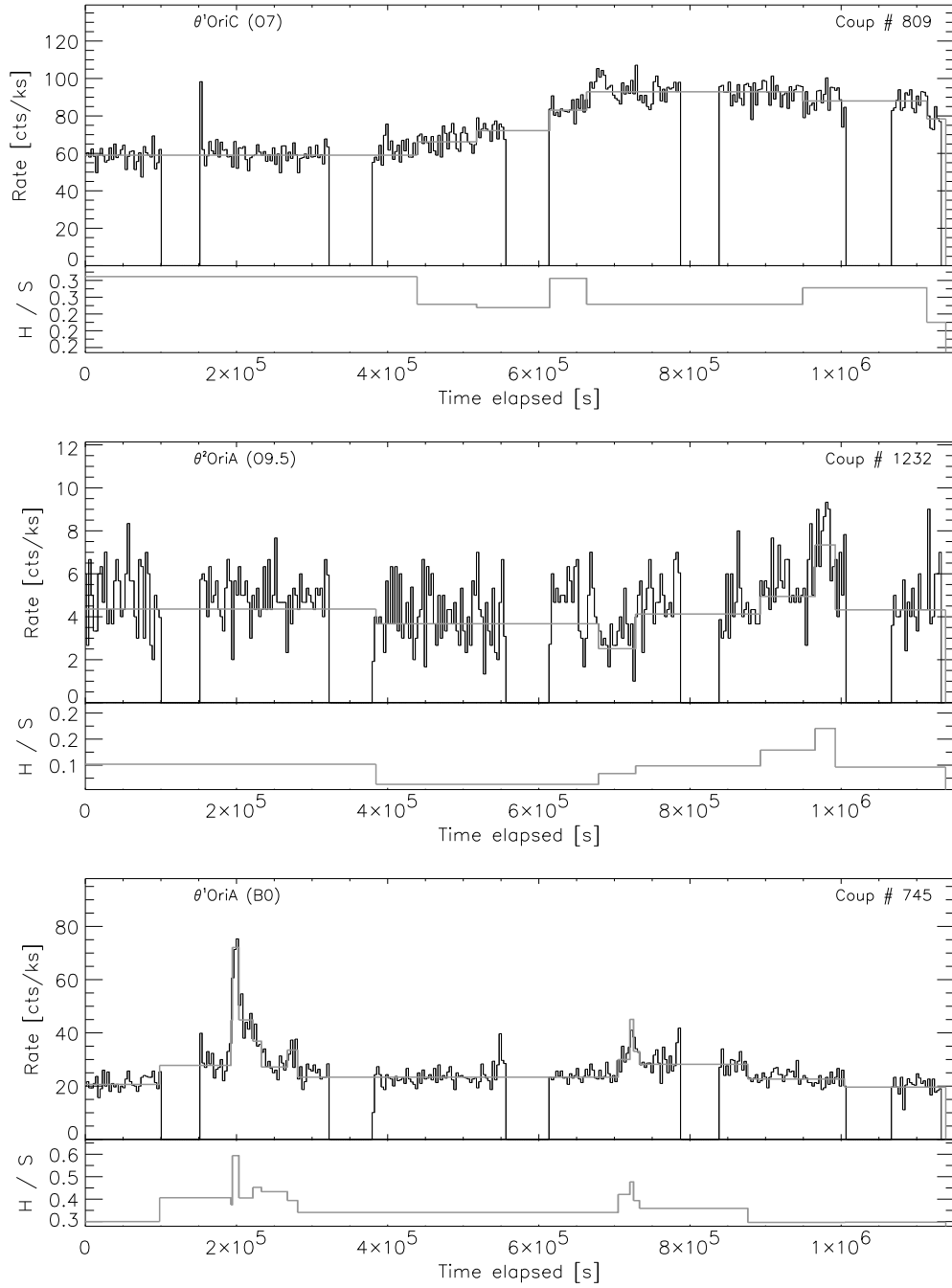
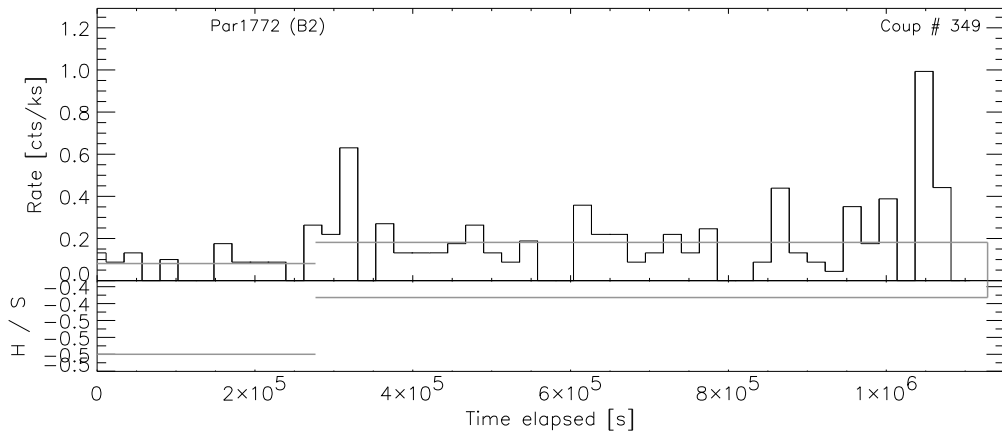
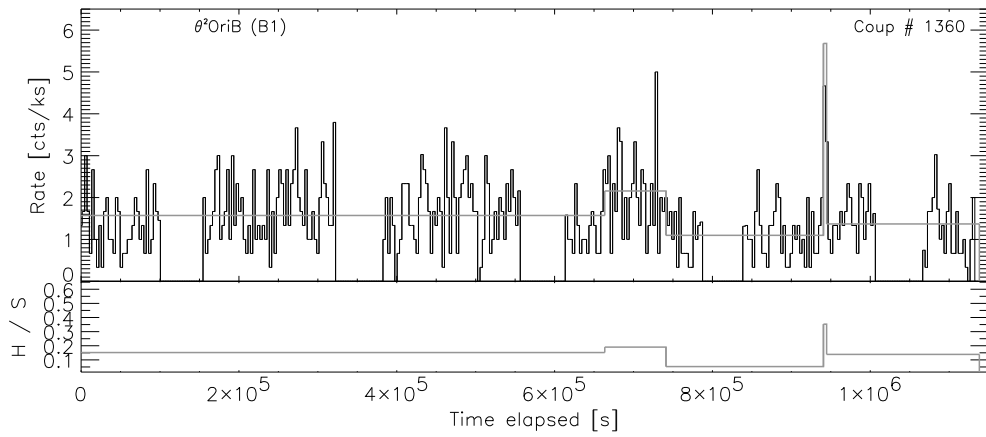
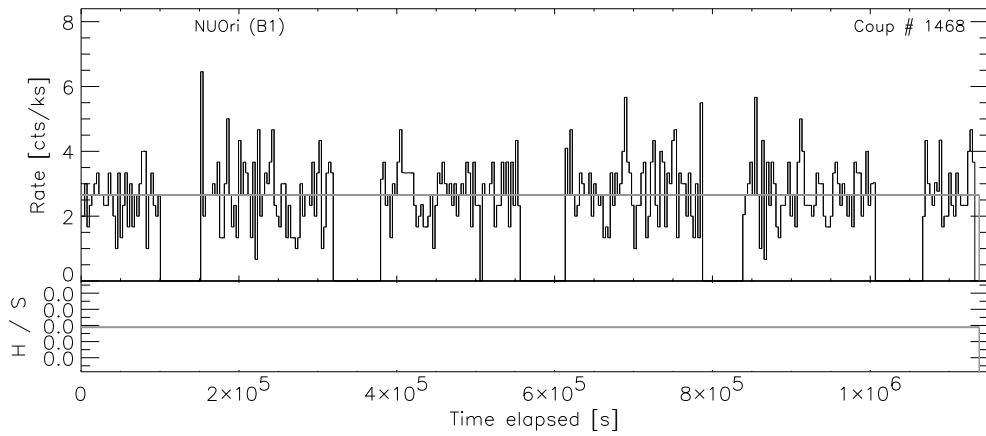
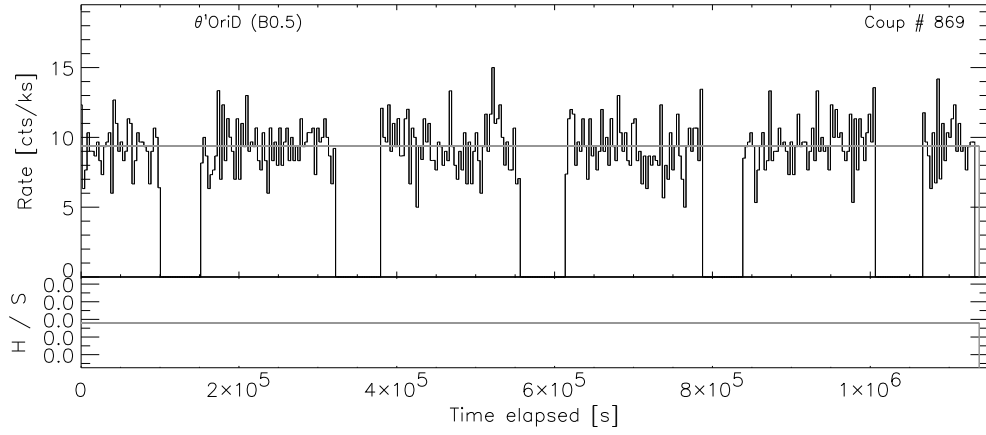
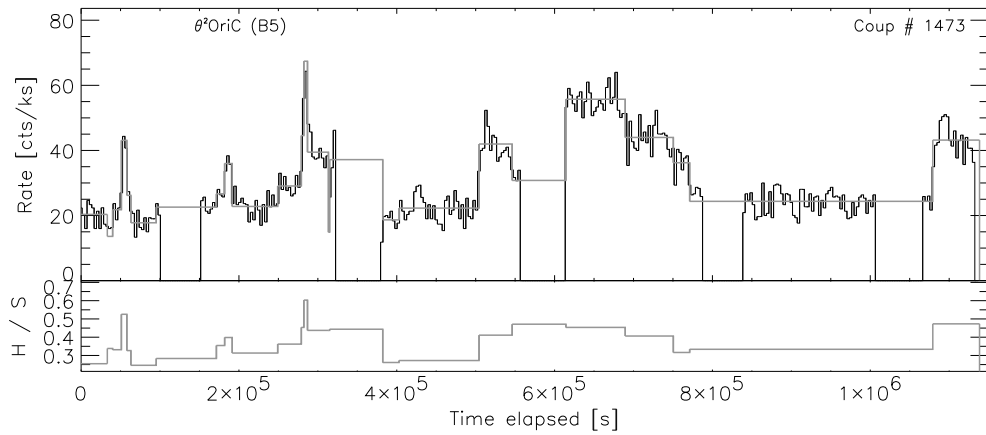
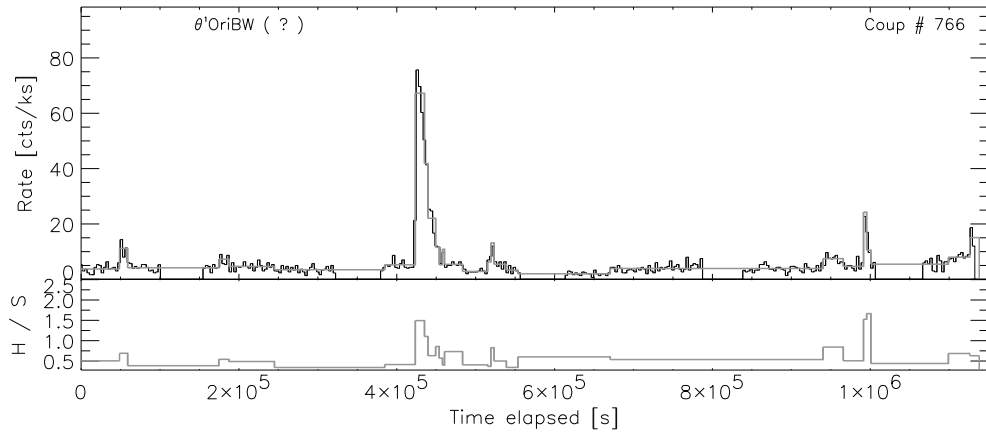
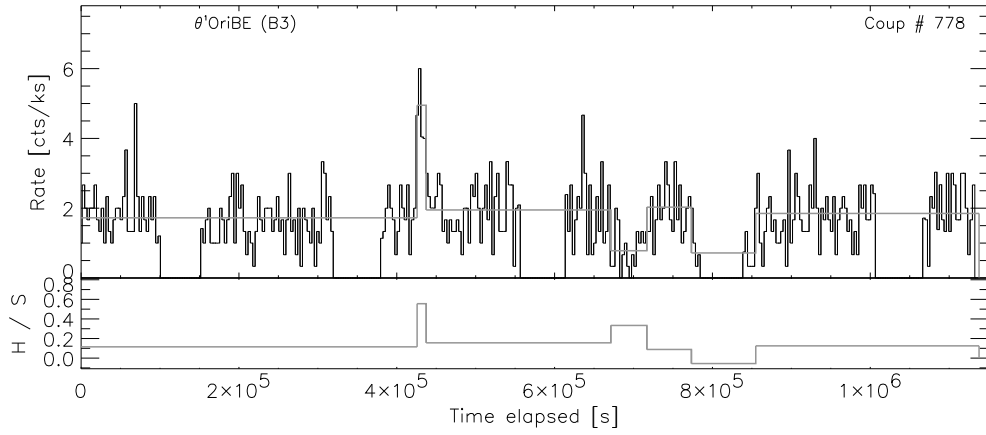
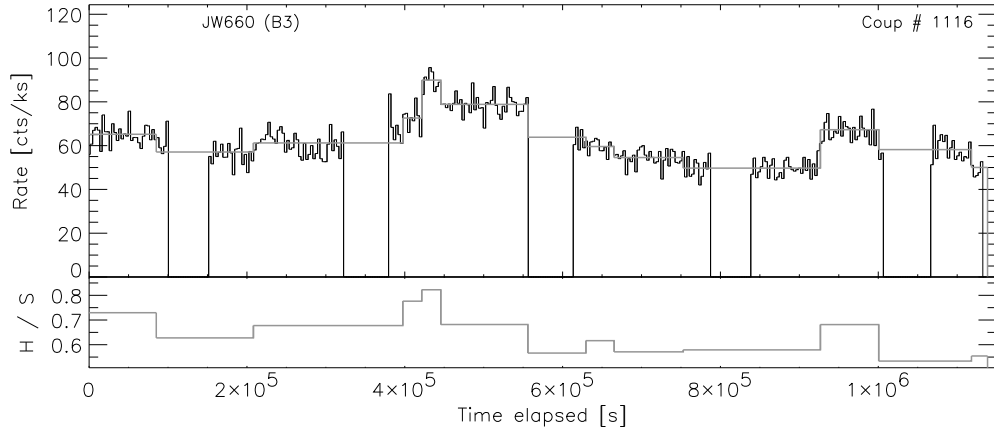
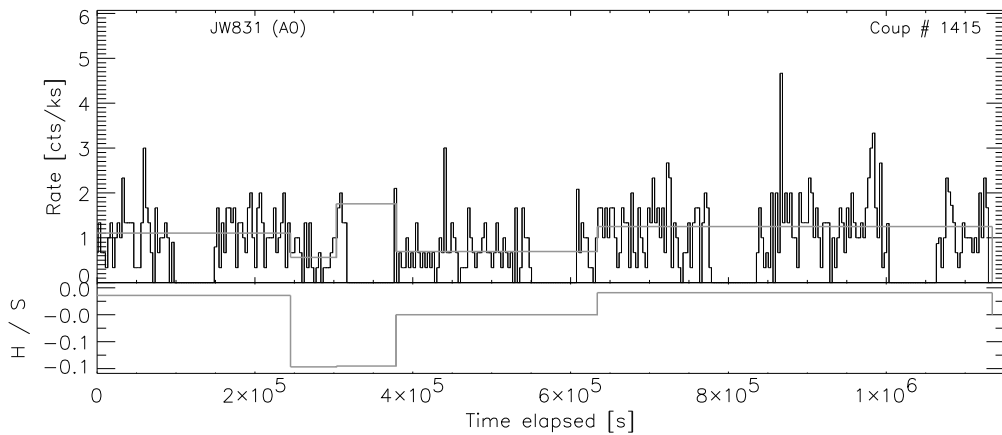
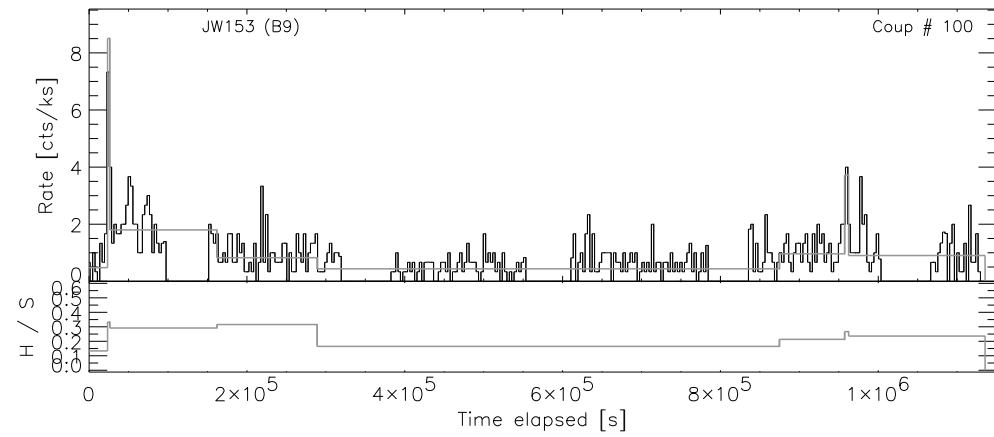
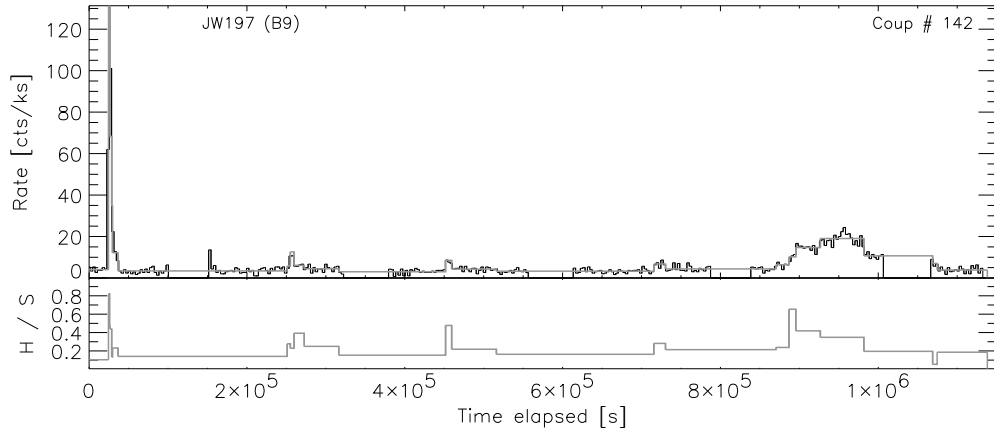
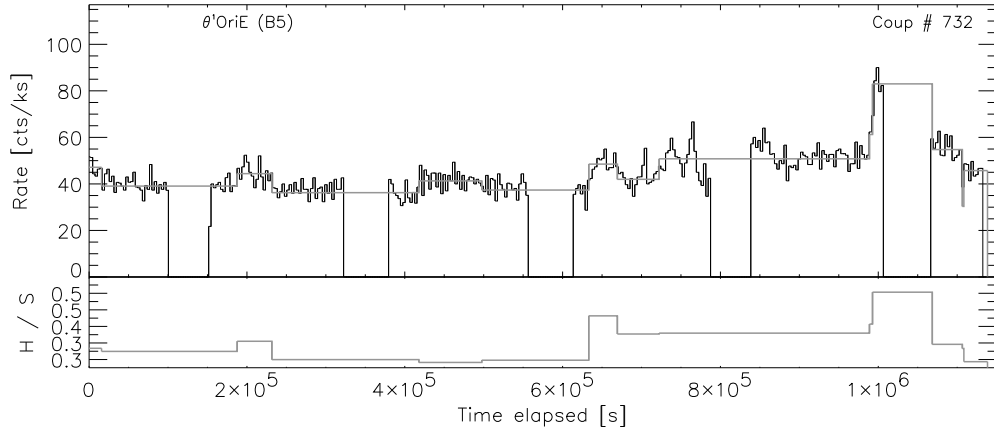


Fig. 5.— Lightcurves of COUP count rate and hardness ratio for detected SW and WW stars in order of decreasing spectral type. Segments derived from the MLB analysis are overplotted with horizontal lines onto the binned lightcurve. The hardness ratios have been evaluated in individual segments.







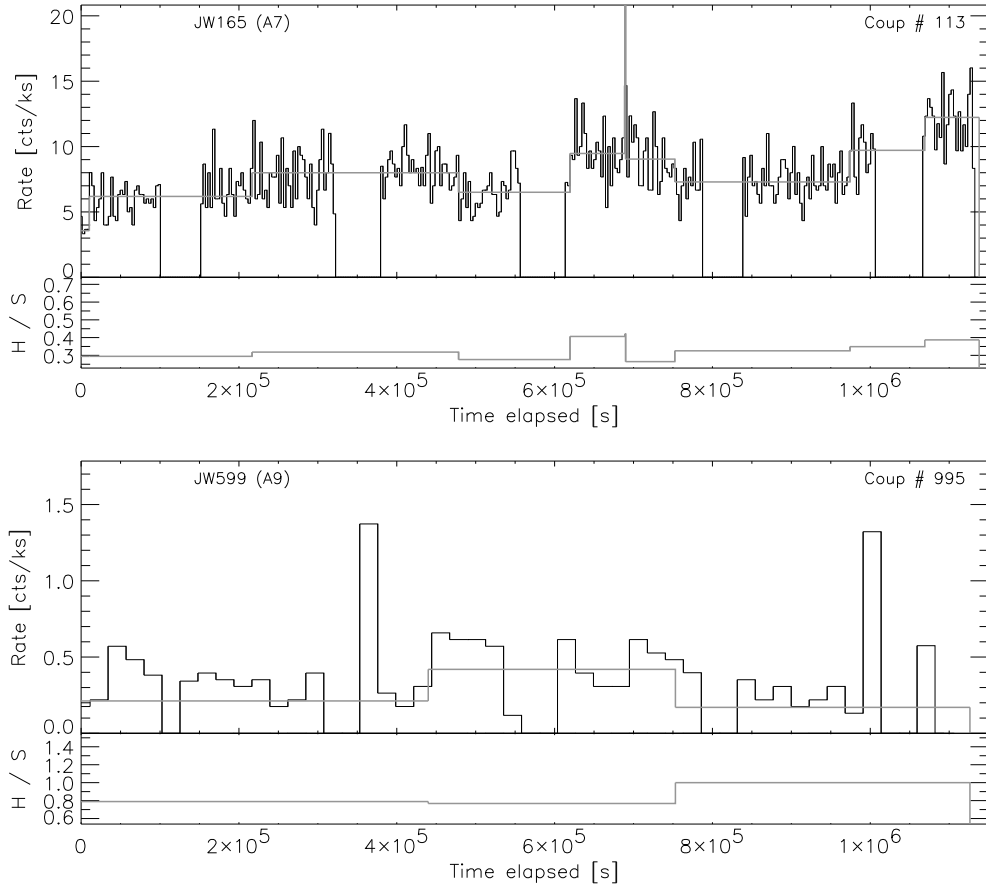


Fig. 5.— *continued*

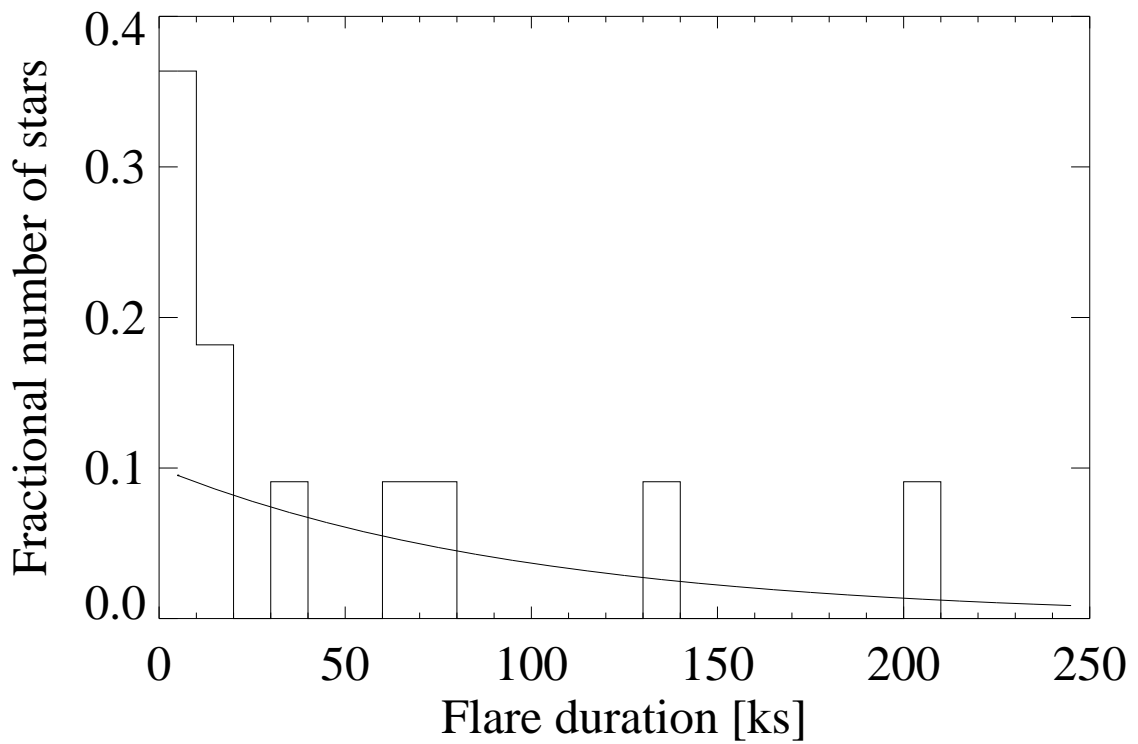


Fig. 6.— Histogram showing the distribution of flare durations for the 11 flares on WW stars. The exponential $0.1 \times e^{(-t/100 \text{ ks})}$ from Wolk et al. (2005) is overlotted.

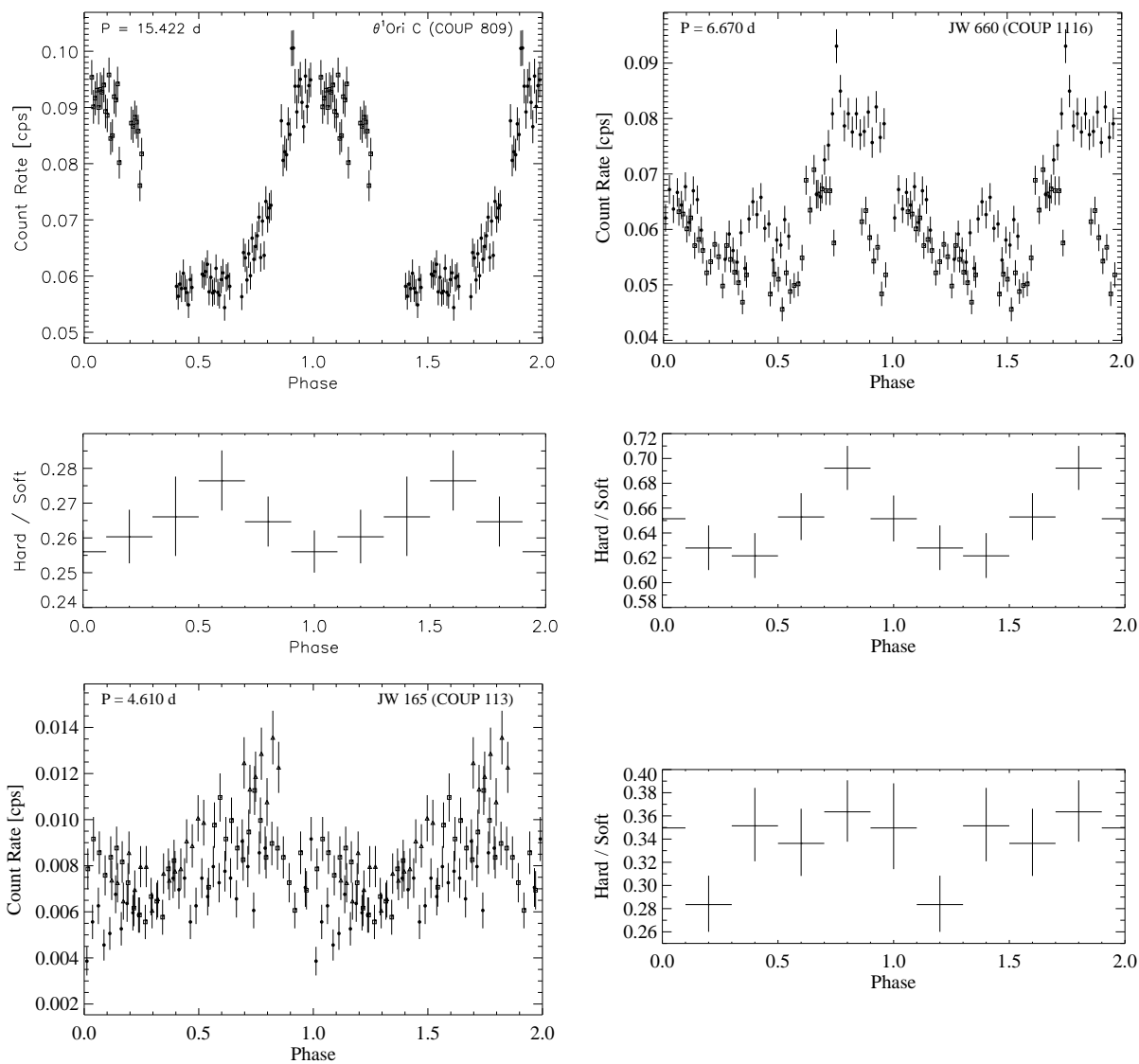


Fig. 7.— Folded X-ray lightcurves and hardness ratios for the three stars with optical photometric periodicities. θ^1 Ori C is folded with the optical period using the ephemeris by Stahl et al. (1996). JW 660 and JW 165 are folded using the period derived from the X-ray data. Data from consecutive cycles are shown with different plotting symbols. The hardness ratio is examined in 5 phase bins.

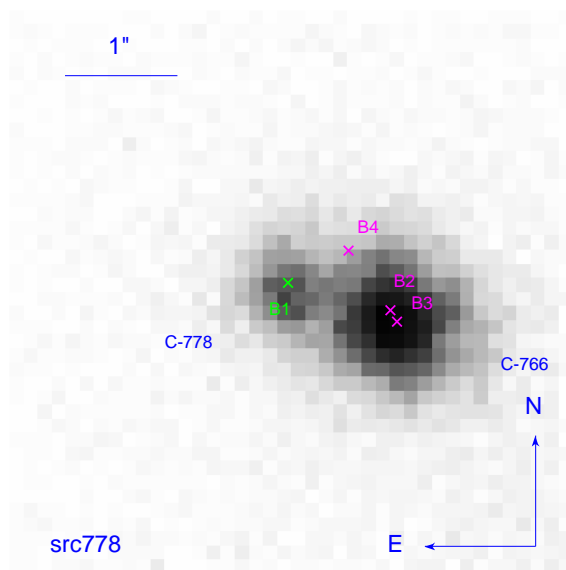


Fig. 8.— COUP image of the region near the θ^1 Ori B quintet displayed at very high resolution ($0.125''$ pixel size). The yellow and magenta \times symbols show the positions of the optical components.

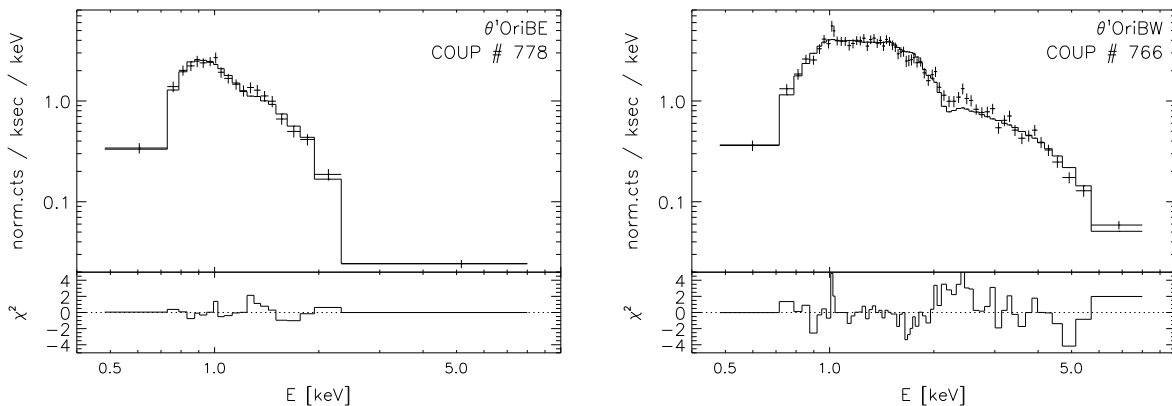


Fig. 9.— ACIS spectra of θ^1 Ori BEast (SpT B3; COUP 778) and θ^1 Ori B West (?; COUP 766). The data are shown with error bars, the continuous histogram is the best-fit model from *XSPEC*, and the bottom panels show residuals between the data and models.

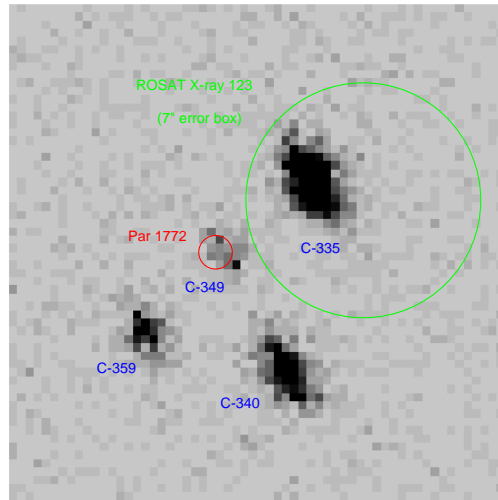


Fig. 10.— COUP image showing the X-ray detection of the B1.5 star Par 1772 (red circle), resolved for the first time in X-rays from adjacent brighter X-ray sources. ‘C-XXX’ denotes the COUP source number, and the green circle shows the *ROSAT* HRC error circle previously associated to Par 1772.

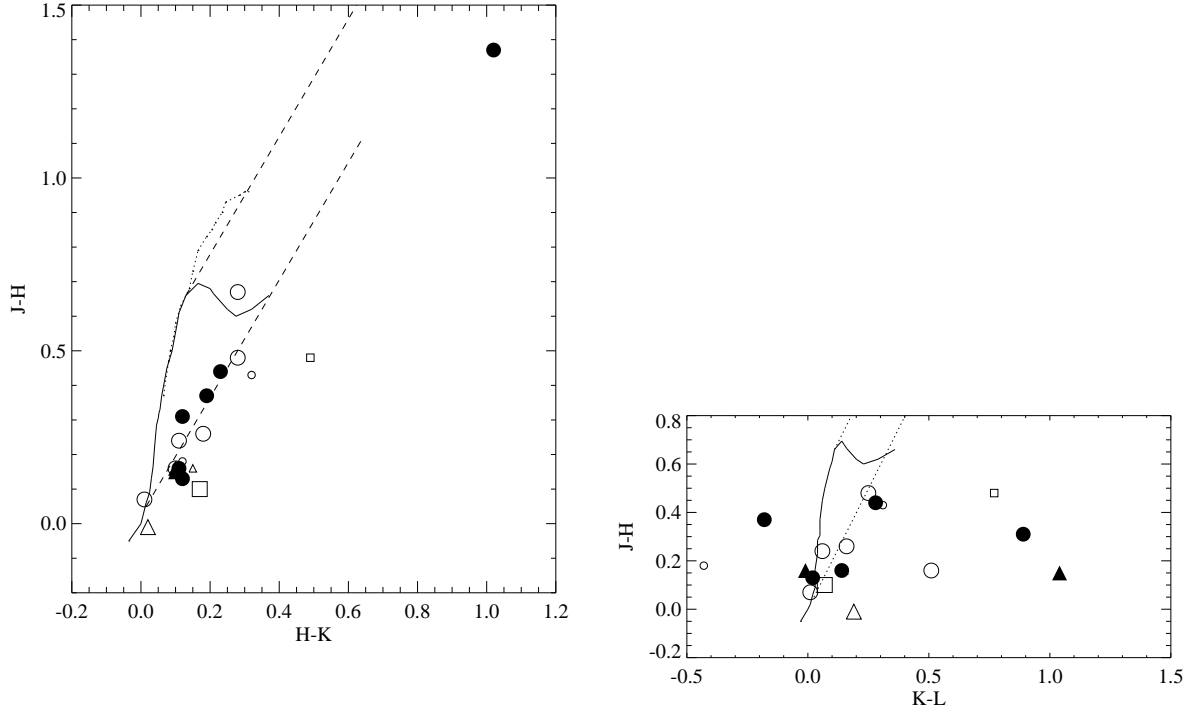


Fig. 11.— Near-IR color-color diagrams for SW and WW stars in the COUP field. Smaller symbols are for stars not detected in the COUP, and filled symbols for known or suspected binaries. Plotting symbols indicate the following properties: *triangles* are *IRAS*-excess stars from Thé et al. (1994), *squares* are chemically peculiar (CP) star candidates from Renson et al. (1991), and *circles* are the remaining normal stars. The solid and the dotted curves are the loci of dwarf and giant stars from Bessel & Brett (1988), and the dashed lines indicate a reddening corresponding to $A_V = 10$ mag using the extinction law by Rieke & Lebofsky (1985).

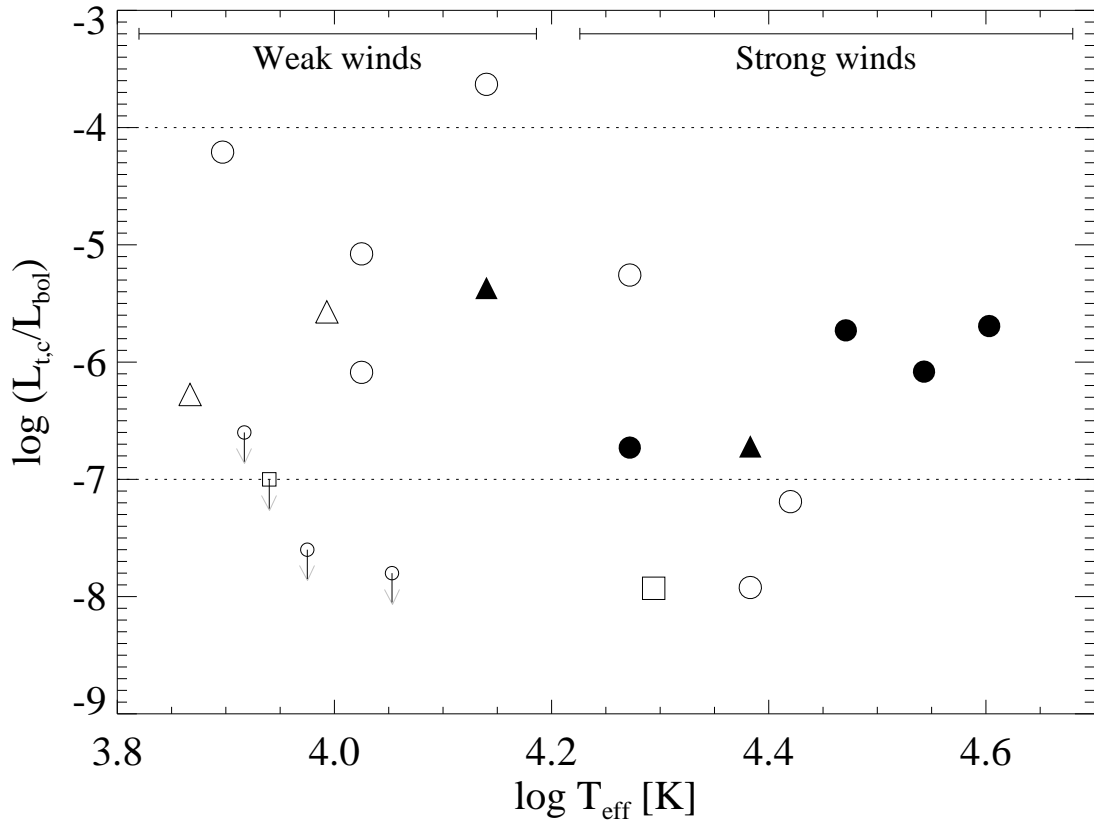


Fig. 12.— X-ray efficiency as a function of effective temperature. The dotted lines indicate the threshold values defined in Sect. 7.1. The plotting symbols are defined in Figure 11.